

# On strain-rate dependent properties of model ice

for simulating ice-induced vibrations

---

Victor Granlund

# On strain-rate dependent properties of model ice

for simulating ice-induced vibrations

**Victor Granlund**

Thesis submitted in fulfillment of the requirements for the  
degree of Master of Science in Technology.  
Helsinki, 22 Jun 2021

Advisor NTNU: professor Knut Høyland  
Advisor Aalto: professor Arttu Polojärvi  
Supervisor: professor Arttu Polojärvi

**Author**

Victor Granlund

**Title**

On strain-rate dependent properties of model ice for simulating ice-induced vibrations

**School** School of Engineering

**Master's programme** Nordic Master in Cold Climate Engineering

**Major** Sea Track

**Supervisor NTNU** professor Knut Vilhelm Høyland

**Supervisor Aalto** professor Arttu Polojärvi

**Level** Master's thesis    **Date** 22.06.2021    **Pages** 53 + 5    **Language** English

**Abstract**

The subject of ice-induced vibrations on bottom-founded vertically sided offshore structures has gained renewed interest with the growth of the offshore wind industry, stimulated by many nations committing to ambitious climate targets. A phenomenological numerical model (Hendrikse 2017) has been developed to predict the occurrence and severity of dynamic interaction events, and Aalto University is involved in the further development of the numerical model, focusing of validation through model scale testing. The numerical model requires calibration based on empirical reference measurements for different types of ice. The work in this thesis includes implementing the numerical model in MATLAB, developing new strategies for increased calibration accuracy, and model scale testing to gather calibration data. This thesis aims to gather insight on the subject of ice crushing in model scale, to arrive at a set of numerical model input parameters that reproduce the behavior of the model ice at Aalto Ice tank, as well as to explore new methods for determining the creep-related input parameters to the numerical model.

A new method for determining creep parameters shows promise, and the results suggest that the cube-root relationship between force and creep velocity previously assumed in the phenomenological model does not apply to model ice, and that Newtonian creep is more accurate. The results also indicate that the model parameters can not be set to mimic delayed-elastic response of ice as measured in a limited indentation test, as it does not yield accurate statistical loads at constant indentation rate tests where ice crushing occurs. The overall calibration effort was unsuccessful due to an unexpected trend between ice velocity and mean global ice load in the continuous brittle failure regime. The trend can not be explained by the phenomenological model, and likely stems from the FG-ED model ice not behaving like natural ice in crushing failure.

**Keywords** Ice-induced vibrations, Numerical modelling, Model scale testing, creep, Burger-Kelvin, Aalto Ice tank, SHIVER

# Contents

<b>Abstract</b>	<b>ii</b>
<b>Contents</b>	<b>iii</b>
<b>1. Introduction</b>	<b>1</b>
<b>2. Modelling ice-induced vibrations</b>	<b>3</b>
2.1 Intermittent Crushing . . . . .	4
2.2 Frequency Lock-In . . . . .	5
2.2.1 Toyama Law . . . . .	6
2.3 Continuous brittle crushing . . . . .	7
2.3.1 Transition from FLI to CBC . . . . .	7
2.4 Creep range . . . . .	8
2.5 Mechanism behind IIV . . . . .	8
2.6 Phenomenological modelling . . . . .	8
2.7 TUD's numerical model for prediction of ice-induced vibrations . . . . .	9
2.7.1 Burger-Kelvin as ice element model . . . . .	10
2.7.2 Crushing against a rigid structure . . . . .	11
2.7.3 Generalizations . . . . .	12
2.7.4 Single element behavior . . . . .	12
2.7.5 Strain-rate effect vs ice edge synchronization . .	14
2.8 Experimental background in IIV . . . . .	14
2.8.1 Experimental validation at HSVA . . . . .	15
2.8.2 SHIVER Pre-tests . . . . .	15
2.9 Model Scale testing . . . . .	15
2.9.1 Scaling ice interaction and crushing . . . . .	16
2.9.2 Aalto Ice Tank . . . . .	16
<b>3. Methods</b>	<b>18</b>
3.1 Previously established method . . . . .	18
3.1.1 Limitations . . . . .	19

3.2	Method applied . . . . .	20
3.2.1	Determining $K_2$ . . . . .	21
3.2.2	Determining $C_2$ by plastic relaxation tests . . . . .	21
3.2.3	Determining $K_1$ & $C_1$ . . . . .	24
3.2.4	Determining $N$ . . . . .	25
3.2.5	Determining $r_{max}$ . . . . .	25
3.2.6	Determining $\delta_{crit}$ . . . . .	26
3.2.7	Parameter fitting . . . . .	26
3.3	Aalto Ice tank test matrix . . . . .	27
3.3.1	Ram structure . . . . .	28
3.4	Overview of code implementation . . . . .	29
3.4.1	Other numerical implementations . . . . .	30
<b>4.</b>	<b>Results</b>	<b>32</b>
4.1	Test data trend . . . . .	32
4.2	Plastic relaxation test and $C_2$ . . . . .	34
4.2.1	Viscoelastic parameters from plastic relaxation .	35
4.3	Ice-structure interaction analysis . . . . .	38
4.3.1	Identifying intermittent crushing . . . . .	38
4.3.2	Identifying resonant lock-in . . . . .	39
4.3.3	Modal analysis of ice-structure interaction . . . . .	39
4.3.4	Buckling and its effects . . . . .	40
4.4	Parameter results . . . . .	41
<b>5.</b>	<b>Discussion</b>	<b>43</b>
5.1	Comparison to pre-tests . . . . .	43
5.2	Plastic relaxation tests in model ice . . . . .	45
5.2.1	Method for determining $F_t$ . . . . .	45
5.2.2	Practicality of plastic relaxation tests . . . . .	46
5.2.3	Accuracy & Uncertainty . . . . .	47
5.2.4	Applicability . . . . .	48
5.3	Calibration results . . . . .	48
5.3.1	SHIVER tests . . . . .	49
<b>6.</b>	<b>Conclusions</b>	<b>50</b>
<b>Bibliography</b>		<b>52</b>
<b>A.</b>	<b>Load means vs. a rigid structure based on single element response</b>	<b>54</b>

<b>B. Link to MATLAB code</b>	<b>57</b>
<b>C. Ram dimensions</b>	<b>58</b>

# 1. Introduction

Ice-induced vibrations have long been a controversial and uncertain subject in the field of ice-mechanics. Ice-induced vibrations may cause severe working conditions, structural fatigue, damage to electronics and machinery, and high global loads. In the famous case of the May 12, 1986 event at Moliqpak [1], severe vibrations by collision with a large ice floe caused a risk of soil liquefaction and sudden catastrophic failure. Ice-induced vibrations have also been the cause of vibrations in structures much smaller than the Moliqpak, such as lighthouses in the Baltic, some of which have failed due to ice loads. The Norströmsgrund lighthouse is an important source of data on IIV, as it has been instrumented with sensors to measure vibration and ice loads, and has since generated a large amount of research and insight in the topic.

There remain unsolved questions regarding the exact physical mechanisms of ice crushing and ice induced vibrations, which cause significant design uncertainties for many offshore projects, especially in fatigue life design. With the growth of the offshore wind industry, the subject has gained renewed research attention. A better understanding of which conditions lead to ice-induced vibrations may allow design buffers for uncertainty to be significantly reduced, hopefully reducing costs and increasing the viability of offshore wind in ice-infested waters.

Recent research at the Delft University of Technology has resulted in a new phenomenological model for simulating dynamic interaction between vertically sided bottom-founded structures and ice. This tool has seen quick uptake by the industry, and work is ongoing to improve and further validate the model. This model is used extensively in this thesis.

The goals of this thesis include finding reference parameters that may be used to simulate ice at Aalto Ice tank, in preparation of an extensive test campaign in the consortium research project SHIVER. This is the first attempt at determining nearly all input parameters for fine-grained ethanol-doped model ice for use in TUD's numerical models. During this calibration effort a new methodology for defining the model creep behavior

is tested. Calibration of the model delayed-elastic response of ice based on the delayed-elastic response as measured in model ice at Aalto ice tank is also attempted, and the merits of this method are discussed.

## 2. Modelling ice-induced vibrations

Three distinct regimes of ice-induced vibrations (IIV) may occur when a level ice sheet collides with a compliant vertically sided offshore structure. These regimes are intermittent crushing (IC), frequency lock-in (FLI), and continuous brittle crushing (CBC). This chapter describes each of the regimes, using visualizations generated with a MATLAB implementation of the TUD phenomenological model for dynamic ice interaction. Sections 2.5, 2.6 and 2.7.1 explore how IIV may be described by a phenomenological model. Later Sections 2.7 and 3.4 provide details and context of this model implementation. Lab as well as field measurements of IC, FLI and CC may be found in literature [2][3].

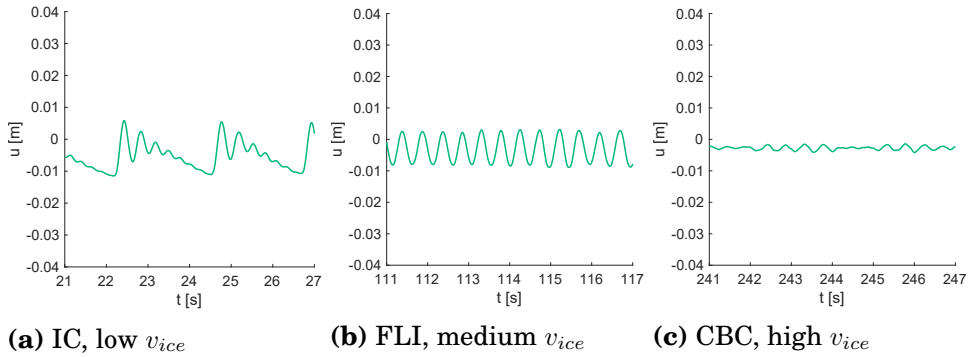


**Figure 2.1.** This simulated structure has an eigenfrequency of 2.11 Hz, and a damping ratio 2% of critical damping.

In Figure 2.1 examples of the three regimes are shown. In this thesis, graphs with a  $u[m]$  axis describe the position relative to rest of a single degree of freedom structure. The position is measured on the waterline, where the ice action is occurring. The ice approaches the structure from the positive direction of  $u$ . In some plots the line is colored according to the magnitude of ice load on the structure at that instant in time. This makes it easy to see how ice load and structure movement are coupled.

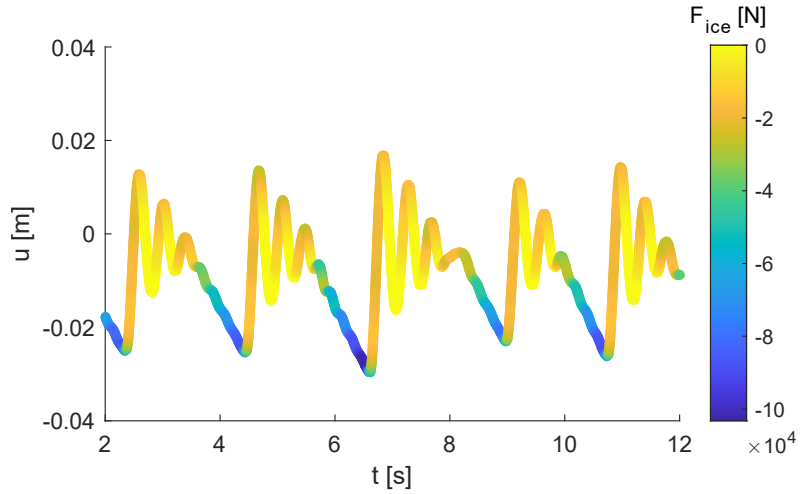


**Figure 2.2.** IC regime causes larger peak loads than FLI and CBC.

## 2.1 Intermittent Crushing

The cycle of intermittent crushing is characterized by a sawtooth pattern in both structural displacement and global ice load. The pattern consists of three phases: loading, unloading, and near-free oscillation. During loading, the true contact area between the ice edge and the structure increases. The increase in contact area is due to local crushing and ductile deformations. Structure compliance is an important factor, as the degree of ice edge synchronization depends on the relative motions of the structure and the ice. The implication is that for a given structure, increasing ice velocity will decrease the peak and average global load during IC, because there is less ductility and less ice edge synchronization.

Hendrikse [4] provides a clear and concise summary of the contact area variation cycle. In loading, the contact area increases until stresses become large enough for a global ice failure. At this stage, almost the entire ice interface fails simultaneously, and the unloading phase begins. The structure makes a jerk toward its rest state, crushing ice on the way. The crushing of ice limits the following transient oscillations, causing the vibrations to be damped. The same crushing of ice is also what separates this oscillating phase from loading. During the loading phase, there is little crushing.

Note that Figure 2.2 is a simulated time series, representing idealized intermittent crushing on the terms of the phenomenological model. Some ignored effects, such as rubble accumulation, may influence the extent of unloading as well as whether the structure reaches rest.

In terms of structural design, dynamic ice actions are primarily relevant to fatigue limit state design, but at slow speeds in the IC range we may find

peak loads that are relevant to global ultimate limit strength design [5]. IIV may also be relevant from an operational point of view, where severe jerking especially during IC unloading may be hazardous to personnel.

An analysis of the temporal ice failure pattern shows that there are distinct periods where little to no crushing occurs. The failure events are not shown in Figure 2.2, but they generally coincide with when the structure is moving against the ice. A part of the transient response is sheltered by the previous oscillation cycle, where some ice has already been broken.

## 2.2 Frequency Lock-In

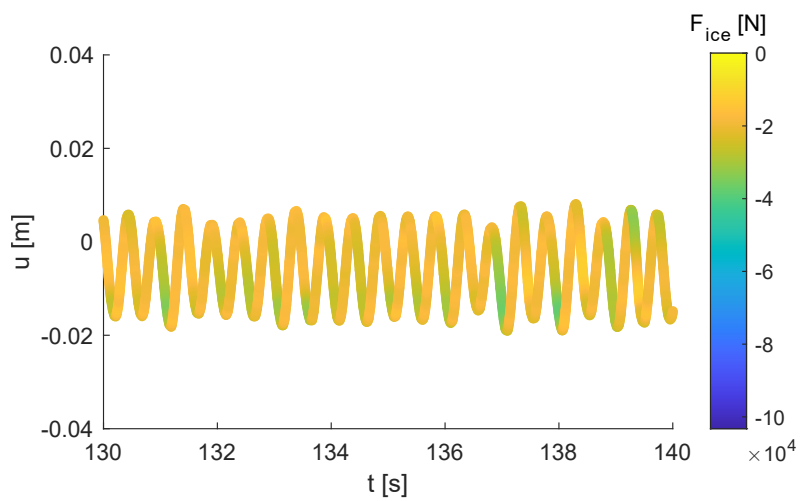


**Figure 2.3.** The structure is vibrating in a sinusoidal pattern in the structural eigenfrequency at 2.1 Hz, a typical example of frequency lock-in.

FLI is characterized by a somewhat stable sinusoidal displacement pattern, as seen in Figure 2.3.

A cycle of crushing failure and elastic ice behavior during FLI has been documented by Toyama [6] among others. Simulation allows the behavior to be visualized easily, as seen in figure 2.4. In general, it is seen that the ice load is larger when the structure is moving with i.e. in phase with the ice. This connection has previously been identified as a "negative damping"-behavior [7]. It can be explained by the brittle behavior of ice under rapid impacts.

In Figure 2.4, where black dots indicate local ice failure, a clear ice failure pattern is seen in FLI, where the rate of crushing depends on the phase of the structural vibration.

After the first peak in Figure 2.4, we see that the structure velocity is near but below ice velocity, which causes a large ice load. However after

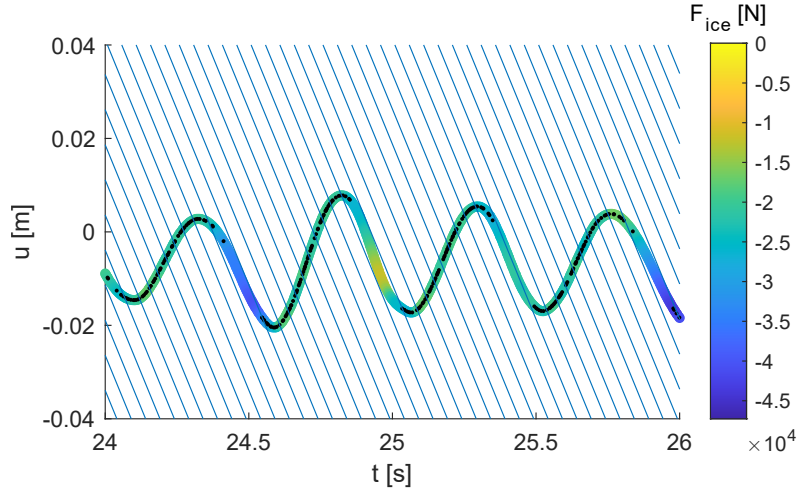


**Figure 2.4.** The black dots along the structural displacement curve indicate that an ice element has failed. The blue sloped lines indicate the movement of the ice, where the slope is equal to the ice velocity. When the slope of the displacement curve is larger than the ice velocity slopes, the force on the structure decreases rapidly.

the following peak, the structural velocity increases above the ice sheet velocity. This is accompanied by a significant drop in ice load. This is at the core of the self-regulation that occurs in steady-state FLI, a self-induced vibration behavior.

### 2.2.1 Toyama Law

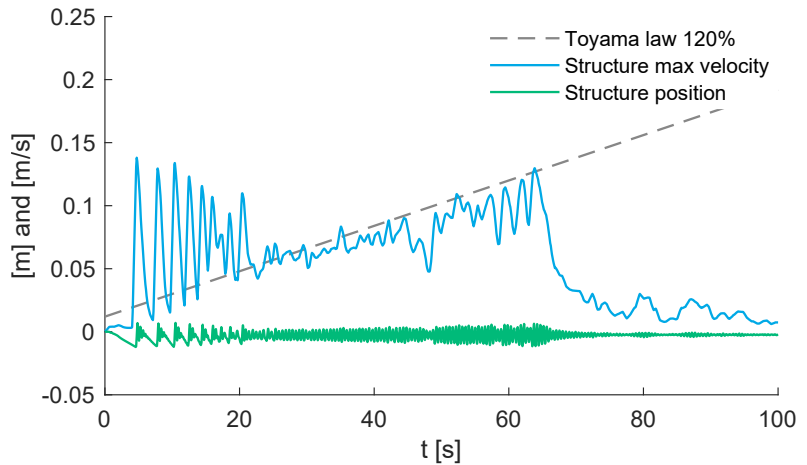


**Figure 2.5.** A simulated scenario where the moving average peak structural velocity during FLI follows  $1.2 * v_{ice}$ , as identified by Toyama. The structure max velocity shown here evaluated as a maximum absolute velocity within a moving interval.

Toyama identified that the peak structural velocity during FLI is usually between 100 % and 150 % of  $v_{ice}$  [6]. This result is reproducible in numerical simulation, as seen in Figure 2.5. A practical implication of this is that when structure is moving with the ice, it may briefly outrun the ice, as was also seen in Figure 2.4. To what extent this occurs depends on the

structural damping, and the relationship of ice force to the properties of the structure. The relationship between peak structural movement and ice velocity is a useful indicator as to whether or not FLI is occurring.

### 2.3 Continuous brittle crushing

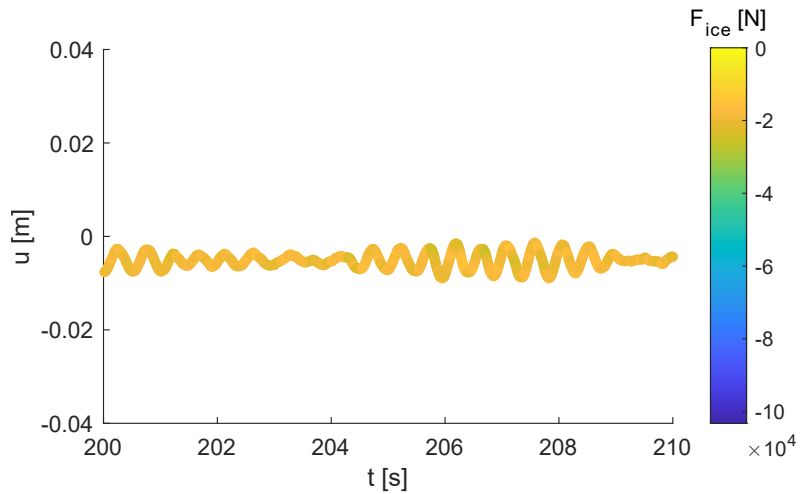


**Figure 2.6.** In CBC, no significant synchronization between structural movement and ice failure occurs.

CBC (Figure 2.6) occurs at large ice velocities. Somewhat counter-intuitively, forces and displacements decrease when the ice velocity increases. The explanation is that the structure movement does not synchronize with ice velocity, thus all contact with the ice leads to a quick brittle failure, not transmitting much load. There is also no time for ice edge synchronization by creep nor by delayed-elastic softening, both of which contribute to loads during IC. When the frequency of ice failure increases, the duration of time associated with every contact event is reduced in proportion or more.

#### 2.3.1 Transition from FLI to CBC

When the structural velocity during FLI becomes large enough for structural damping to overcome the excitation force, FLI transitions to CBC. The excitation in FLI is dependent on the synchronization of structure movement with ice velocity, thus the self-induced feedback loop is broken. This suggests that for a given structure stiffness and mass, the critical velocity at which self-excited FLI may occur is a function of structural damping and ice conditions. Weakening the ice, or conversely increasing the structural damping both decrease the magnitude of the

critical velocity.

## 2.4 Creep range

In summary of IIV: IC happens at low  $v_{ice}$ , FLI at medium  $v_{ice}$ , and CBC at high  $v_{ice}$ . At very low ice velocity, below the creep transition velocity  $v_t$ , there is a fourth mode of interaction, where plastic creep will prevent any sudden failure of the ice. This is a quasi-static mode of interaction, i.e. not IIV, however the phenomenological model does support this mode of interaction. In principle, plastic flow plays a part in the failure of ice at any ice velocity, however the effects may be negligible especially in the range of FLI  $v_{ice}$ .

## 2.5 Mechanism behind IIV

For large nominal ice contact area aspect ratios, ice brittleness increases as strain-rate increases. Much research has been done on this subject, and the ductile to brittle transition (separate from the transition to complete creep failure) is well documented in Schulson [8]. He acknowledges strain-rate softening, which is a key phenomenon in especially FLI. At high strain-rates, spalling or splitting phenomena dominate, while at low speeds local microcracking and ductile deformations occur before spalling. These microfailures that occur before large scale failure increase the area of the ice-structure interface, as well as prolong the duration before failure of the local ice action.

Previous theories for predicting IIV, like the negative damping theory by Määttänen mentioned in Section 2.2, have incorporated strain-rate brittleness as a key phenomenon, but do not include contact area variation, which has been confirmed by Sodhi [9] to occur during IC. The description of ice behavior during IIV is clearly incomplete without contact area variation.

## 2.6 Phenomenological modelling

A phenomenological model is the basis for the simulations in this thesis. It is important to understand that while a phenomenological model may emulate reality very well, it is not derived directly from physical nature. For example, each ice element does not have a specific length or width or

area or even shape, it does not have a physical equivalent. However the synchronization of these elements is analogous to contact area variation. The model is designed to behave like the contact area variation, but it's meant to be a complete description of contact area variation.

It is useful to keep the model simple and focused to a single purpose. Many phenomenological models must be tuned empirically, and this becomes more difficult to do when the number of variables increases. The flipside of simplicity is limited applicability, thus it is vital that the user of a phenomenological model understands the limits of the generalizations made.

## 2.7 TUD's numerical model for prediction of ice-induced vibrations

The phenomenological model for ice loads on a vertical structure employed in this thesis was first presented by Hendrikse in 2015 [4]. The latest iteration is presented in [10], along with a MATLAB example implementation. A rough overview is shown in Figure 2.7, and the ice elements are described in Section 2.7.1.

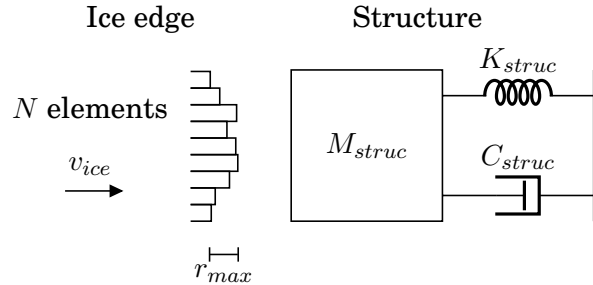


**Figure 2.7.** An overview of the simulation parts, displaying an ice edge as a number of elements. In this case, a single degree-of-freedom structure representation is used.

The phenomenological model contains 7 input variables, of which the number of elements  $N$  and the maximum element spawn distance  $r_{max}$  are seen in Figure 2.7.  $K_1$ ,  $K_2$ ,  $C_1$  and  $C_2$  may be seen in a schematic drawing in Figure 2.8, and together with failure criterion  $\delta_{crit}$ , they constitute a description of a single ice element.  $r_{max}$  influences the load variation, as elements spawn randomly within a uniform distribution between zero and  $r_{max}$  distance from the structure. Note that for a given  $v_{ice}$ ,  $N$  and  $r_{max}$  also control the frequency with which the structure encounters ice elements.

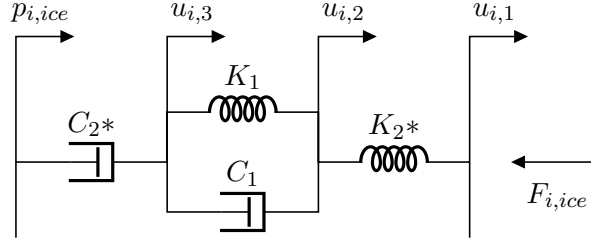


**Figure 2.8.** A schematic drawing of a Burger-Kelvin type element. The asterisk indicates nonlinearity.  $K_2$  is nonlinear only in the sense that it may not act in tension, while the creep behavior is nonlinear with regard to the force acting over the element.

### 2.7.1 Burger-Kelvin as ice element model

A Burger-Kelvin (BK) element, i.e. a Kelvin representation of a Burger material, consists of a pure elastic spring, a viscoelastic spring, and a dampener connected in series. In a slow compression scenario, the viscous part of the viscoelastic element is weak, and thus the element will act like a series of elastic springs, which move in equilibrium with each other. The ratio of  $K_1$  to  $K_2$  determines which of the elastic and viscoelastic components is compressed more. In a rapid compression scenario, the viscous damper will prevent compression of the middle component, and the pure elastic spring will take all the compression. Regardless of the relative quantities of  $K_1$  to  $K_2$ , increased damping will always make the element modulus larger for rapid compression compared to slow compression.

The ice elements used in the model include a few modifications from the basic BK-material, the foremost of which is a failure criterion for the element. The failure criteria is a critical deformation in the pure elastic component. In effect, this is the same thing as a limit force criteria, because all three components are coupled in series, and the same magnitude of force will always be acting over each component. The failure criteria is given by Equation 2.1.

$$F_{element} > K_2 \delta_{crit} \quad (2.1)$$

The maximum global ice load from full element synchronization (where all  $N$  elements are in contact with the structure) is given by Equation 2.2:

$$F_t = \max F_{ice} = N K_2 \delta_{crit} \quad (2.2)$$

The second modification to the base BK-element is that the creep component (rear dampener) is nonlinear, so that the behavior in creep follows the power-law creep behavior of ice more accurately. The force over the

creep component is given by Equation 2.3

$$F_{creep} = \dot{u}_{creep}^{1/3} C_2^{1/3} \quad (2.3)$$

The element may never act in tension on the structure. Cases where the element is unloaded and loses contact with the structure must be handled, where the viscoelastic component will take some time to return to rest. The choices behind the element representation are motivated by Hendrikse in [10].

### 2.7.2 Crushing against a rigid structure

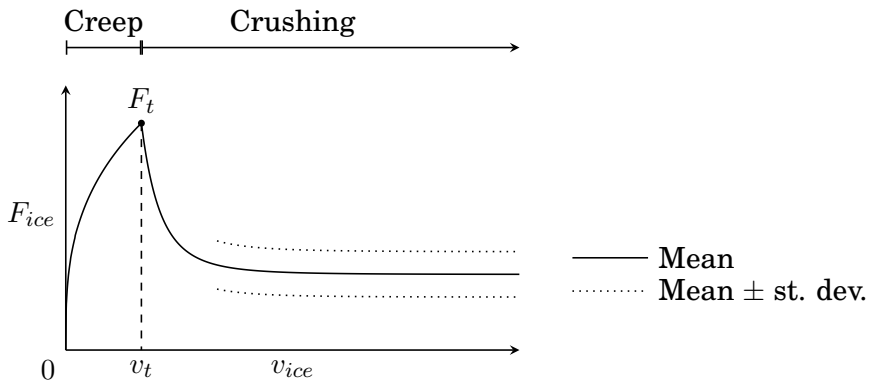


**Figure 2.9.** The crushing load mean and variance as functions of ice velocity are shown. All parameters ( $N$ ,  $K_2$ ,  $K_1$ ,  $C_1$ ,  $C_2$ ,  $r_{max}$ , and  $\delta_{crit}$ ) affect the shape of these trends, and only a few points on this curve can be calculated analytically. This figure is revisited and presented in additional detail in Section 3.1.

The model consists of the parts presented in Sections 2.7 and 2.7.1, and this section covers the general behavior of the model as applied to crushing against a rigid structure. The case of crushing against a rigid structure is useful as the dynamic interaction between structure and ice, which is what we usually try to capture with the model, is eliminated which removes structural properties from the equations.

The load trends as functions of ice velocity are presented in Figure 2.9. Observe that above creep transition velocity  $v_t$ , mean loads decrease when indentation velocities are increased. This is due to increasing brittleness in element behavior, as the increased strain-rate causes elements to be stiff and fail earlier, decreasing both the mean load during the element lifetime as well as the mean contact ratio, which is the percentage of elements that contact the structure at any point in time.

At any speed above transition velocity  $v_t$ , only CBC will occur, as no temporal synchronization of ice failure can occur without structural compliance. In reality, there are no completely rigid structures, but there may be

ratios of ice load to structural stiffness where it is completely reasonable to neglect structural compliance.

The case of crushing against a rigid structure is what is used to determine model input parameters, as having negligible load contributions from dynamic interaction reduces the number of variables during the calibration process.

### 2.7.3 Generalizations

Ice crushing is very chaotic by nature, which should be reflected in the model. The only source of randomness in the model is the placement of new elements within  $[0, r_{max}]$  distance from the structure. In order to empirically tune the model behavior such that it properly reflects the randomness of ice as a material, one might have to exaggerate  $r_{max}$  when calibrating parameters. This also implies that  $r_{max}$  may not be a physically measurable quantity, as that calibration strategy might overly constrain the viable parameter solution space.

Some of the parameters do not accurately reflect the inhomogenous nature of natural ice, as they are constant values. For example, it has been estimated in [11] that the value of  $\delta_{crit}$  follows a probability function reminiscent of a Poisson-distribution with a long tail. It is also fair to assume that the other parameters related to element strength and element number are not constants, like the model assumes, but should be picked from a distribution.

These generalizations reduce the randomness of the interaction. For the purposes of investigating IIV, this is not a big issue, as these are steady-state type interactions that mainly affect design from a fatigue perspective, and the idealized nature only makes the predictions a bit conservative. However, if design peak loads were also based on a single fully synchronized IC-event, which may cause very large loads, this model would not be sufficient to predict that peak load for e.g. ULS design. The importance of understanding the limitations to the applicability of any phenomenological model must not be understated.

### 2.7.4 Single element behavior

The response of individual ice elements is easiest understood through visualization, and this subsection includes some examples.

Figure 2.10 depicts the element response as a function of time, where

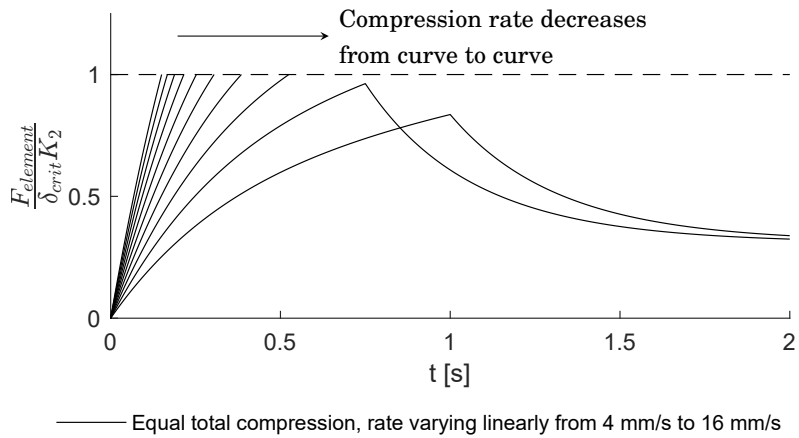


**Figure 2.10.** Due to delayed-elastic response and creep, compression rate has a strong effect on the impulse per element failure. Each curve corresponds to a different compression rate (albeit reaching the same cumulative compression), the higher velocities having more linear stress/strain-curves while slower rates fail later, having greater mean loads during their element lifetimes.

each curve corresponds to a different rate of compression. As compression rates decrease from curve to curve, elements fail later and with a greater mean load during their element lifetimes. Also note that the slowest two compression rates do not reach the force failure criteria whatsoever, despite equal total element compression under each of the compression rates. Once delayed-elastic response has ran its course, both non-broken elements settle to the same load level.

Observe that for a decrease in ice velocity, the encounter frequency (the rate at which ice elements impact the structure) decreases, but the duration of time that an element stays in contact with the structure increases faster than the encounter frequency decreases. This leads to an increase in mean ice load when ice velocity is decreased.

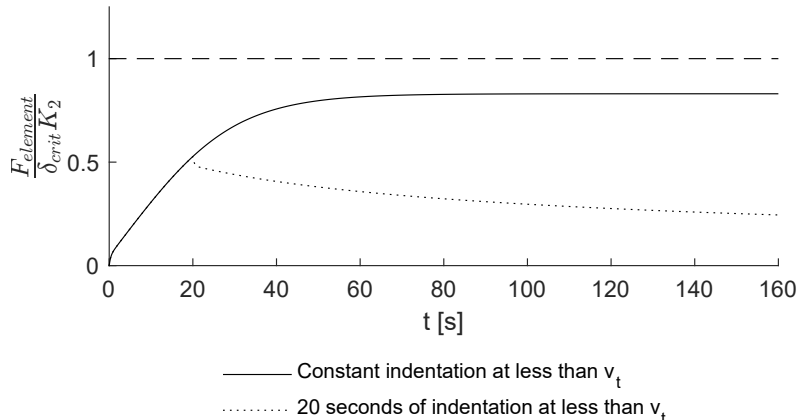


**Figure 2.11.** In this longer timeframe the effect of creep on a single element is seen.

In Figure 2.11 two curves are shown. The constant indentation rate curve shows what happens at indentation speeds below transition velocity,

where creep prevents the element from local brittle failure. The dotted curve depicts the element behavior in a scenario where indentation stops, and the element load dissipates due to creep relaxing the elastic springs in the element.

### 2.7.5 Strain-rate effect vs ice edge synchronization

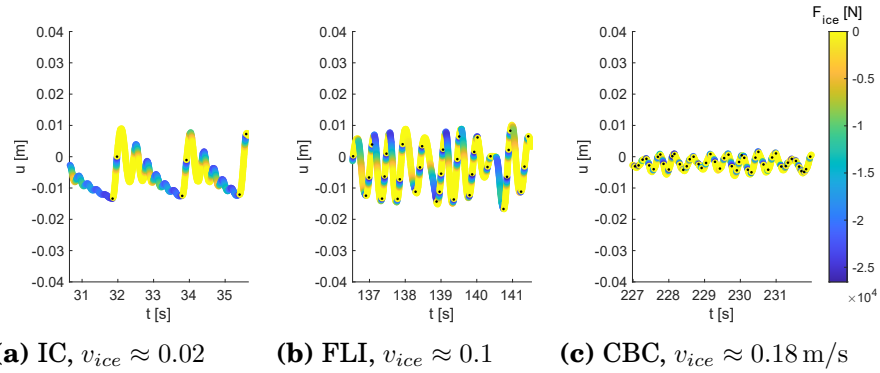


**Figure 2.12.** Simulated using  $N = 1$ , where the element strength parameters have been increased accordingly. We see that we get roughly similar structural response, but in FLI and CBC (where little synchronization would usually occur) minimum and peak loads are inaccurate. Mean loads can be somewhat accurate.

In theory, the synchronization of elements due to structural movement is not a necessary condition to get all the modes of IIV. With our element failure criteria, the Burger-Kelvin element (shown in figure 2.8) is weak in rapid compression, and strong for slow impacts, which is a base condition for the self-induced nature of FLI.

For demonstration purposes, a single element simulation was made. Ice edge synchronization doesn't occur if there is only a single element. From figure 2.12 it is seen that the simulation has reproduced all the regimes of IIV, but the variation around the mean load has increased especially in FLI and CBC. Thus the number of elements strongly affects load variance. By analyzing the range of temporal load variation during CBC, we may determine the appropriate number of simulation ice elements given a load timeseries.

## 2.8 Experimental background in IIV

This section shortly covers work done to validate the numerical model at HSVA as well as results from SHIVER pre-tests, both of which provided valuable information for planning our test matrix.

### 2.8.1 Experimental validation at HSVA

TUD:s phenomenological model has been validated at HSVA in model scale tests. Tests were performed using a structure with an adjustable level of compliance, so both rigid indenter tests for determining model input parameters and actual IIV tests could be performed with the same structure. The IIV tests could then be resimulated in order to verify that the model does yield an accurate prediction of IIV in model scale. There were some issues with unwanted ice flexure, due to which good similarity between tests and simulation could not be achieved for the IC regime [11]. Any hints of buckling or flexural failure must be looked out for during our tests, as the target ice conditions or the structure should be adjusted to eliminate these unwanted failure modes.

### 2.8.2 SHIVER Pre-tests

Pre-tests for the SHIVER test campaign were performed at AIT in February 2020, and a cylindrical ram was used to perform crushing tests at various speeds in a range of ice conditions. The purpose of this was to find target model ice conditions that produce ideal IIV, where buckling is kept to a minimum and the crushing process has the right characteristics, such as the size of ice fractures, generated type of rubble, means and peak loads. The target ice conditions for the planned SHIVER test campaign 2021 at AIT are based on these pre-tests, and as the initial plan was that the parameter findings of this thesis will be verifiable based on the data from the upcoming test campaign, and that the same target ice conditions should be used.

## 2.9 Model Scale testing

Model scale testing is usually a useful prototyping tool for e.g. specifying power output for ice-going vessels. In such experiments, it's important to use analytically sound and experimentally proven scaling laws that preserve the accuracy of a prioritized property, usually some dimensionless number. For testing icebreaking hulls, Froude and Cauchy numbers are usually preserved, as well as the ratio of inertial forces to flexural strength of ice.

Our tests at AIT consider the inverted problem. Instead of e.g. testing

some type of structure to see the ice loads for that structure, we focus on testing the ice in a way that eliminates as many factors from the structure as possible. This way, we can hopefully learn to simulate the ice accurately.

### 2.9.1 Scaling ice interaction and crushing

There is no established precedent for scaling crushing behaviour. Time scaling is necessary in order to preserve eigenfrequencies when scaling down structures, but the strain-rate dependent strength of ice does not scale, and thus this property is incompatible with time scaling. The scaling up of measured model scale results is thus an unsolved and highly complex problem. In effect, this means that it is not known what the full-scale equivalents of the model-scale tests are.

In the context of determining model inputs, a rigid indenter is used and thus the scaling of eigenfrequencies is not an issue. However the inputs must be determined within the same scaling preconditions as for the SHIVER tests, where the solution to preserving eigenfrequencies in scaling has been to replace the structure with a robot, artificially controlling the structural vibrations, eliminating the need for time-scaling. Note that this thesis does not attempt or require any scaling of model test data, and thus no further attention is paid to the subject.

### 2.9.2 Aalto Ice Tank



**Figure 2.13.** Aalto Ice tank and the unbroken ice sheet used for our tests.

Aalto Ice Tank (AIT) is a 40 x 40 m model ice basin in Otaniemi, Espoo. The ice is fine grained ethanol doped. The types of tests typically performed at AIT include towed ice resistance tests for ship hulls, self-propelled tests in ice, as well as maneuvering tests. The width of the basin makes it very

versatile, and the inclusion of wave-makers make the tank useful for a range of open water type in addition to model ice experiments.

Following ice spraying and freezing, the ice is usually tempered, which weakens the ice in order to attain an accurate scaled strength value. Based on SHIVER pre-tests at AIT in February of 2020, untempered ice gives us the most accurate crushing behavior. There is a length-scale to the spalling/cracking behavior, and changing the hardness of the ice is one way to influence the length-scale. Whether the behavior is accurate or not may be judged based on the load pattern, the size of the ice fractures, and the amount of plastic flow, as well as the general load trends.

One issue with the AIT ice is a vertical strength gradient in the ice. There is a near-linear strength relation, where the ice is quite hard at the top, but very mushy on the bottom, which can be easily verified by scraping a chunk of the ice with a sharp instrument. The process of tempering would weaken the relative strength gradient (Personal communication, Teemu Päivärinta 26.1.2021), but as the ice for our tests is not tempered, attention must be paid to observe any unwanted buckling or flexing that may occur as a result of the strong strength gradient.

Note that a strength gradient is normally found in natural ice as well, owing to temperature, brine, porosity and grain-size distributions.

### 3. Methods

The phenomenological model is not based on any standard physical material properties of ice, and must therefore be calibrated via empirical reference measurements. This chapter presents the methods for determining those simulation input parameters for a model scale reference case. The methods for determining  $C_2$  are new, and the rest is based on methods presented by Hendrikse [10]. This chapter also describes the model scale tests as well as details about the code implementation used in this thesis.

#### 3.1 Previously established method

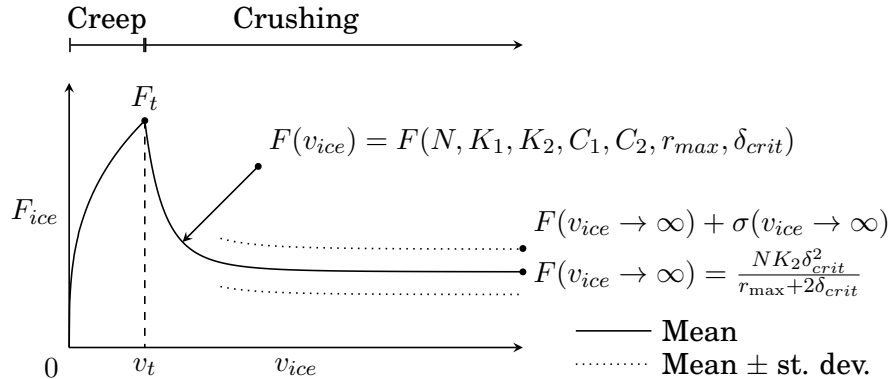


**Figure 3.1.** This figure describes the general force trends against a fully rigid structure. Some points may be described analytically, and are thus important calibration values to be measured.

According to Hendrikse [10], a valid calibration shall fulfill a system of analytical equations describing the statistical behavior of the model against a rigid structure, where  $F_t$  (at  $v_t$ ),  $F(v_{ice} \rightarrow \infty)$ ,  $\sigma(v_{ice} \rightarrow \infty)$  as seen in Figure 3.1 are measured empirically. The system of equations is given in Equation 3.1.

$$\begin{aligned}
\delta_{crit} &= \delta_{crit} \\
r_{max} &= \delta_{crit} \left( \frac{F_t}{F(v_{ice} \rightarrow \infty)} - 2 \right) \\
N &= \frac{\frac{2F_t}{3F(v_{ice} \rightarrow \infty)} - 1}{\left( \frac{\sigma(v_{ice} \rightarrow \infty)}{F(v_{ice} \rightarrow \infty)} \right)^2} \\
K_2 &= \frac{F_t}{\delta_{crit} N} \\
C_2 &= \frac{F_t^3}{N^3 v_t}
\end{aligned} \tag{3.1}$$

Note that  $\delta_{crit}$  isn't a parameter that we find by fitting, it's simply assumed, e.g. based on literature. The same is true for  $v_t$ , which is not an input parameter but an important data source calibration. Measuring or estimating  $v_t$  is not trivial.

The last two parameters  $C_1$  and  $K_1$  must be solved by iteratively fitting simulated mean forces ( $F(v_{ice}) = F(N, K_1, K_2, C_1, C_2, r_{max}, \delta_{crit})$ ) at one or more ice velocities above  $v_t$  yet slow enough that delayed-elastic response makes  $F(v_{ice}) > F(v_{ice} \rightarrow \infty)$ .

Figure 3.1 is a simplification of the real mean trend at ice velocities just above transition velocity, there is what may be described as a hump in the trend, with a magnitude and center (in terms of ice velocity) that depends primarily on the relative magnitude of  $C_1$  and the ratio of  $K_1/K_2$ . This hump is presented in Appendix A, and hasn't been presented earlier literature.

### 3.1.1 Limitations

The basic calibration methodology requires that the test structure is sufficiently rigid or massive that negligible dynamic interaction occurs. In practice, this is difficult to achieve, especially at low velocities where loads will be large.

In order to quantify  $C_2$ , it is necessary to perform runs at very slow indentation velocities. With the regular equipment at ice towing tanks, this may not be possible, especially at the load level required. At AIT, it is not possible to move the wagon at a slower speed than 10 mm/s, whereas  $v_t$  may be below 1 mm/s. Thus it's not possible to get measurements near  $F_t$  via indenter-tests.  $C_2$  has usually been calculated from an assumed  $F_t$  at an assumed  $v_t$ , with an assumed power-law behavior.

### 3.2 Method applied

This section describes the process in detail for determining each ice input variable, as applied in this thesis at AIT. The relative proportions of the parameters affect the statistical behavior of the model. Some of these statistical measures can be inferred analytically, and some can only be found by running the code. The statistical behavior includes properties such as mean loads, load variance, peak loads, mean element failure rates, and the behavior should be statistically accurate at all ice speeds.

There is a lot of information in this section, but the general steps in calibration are quite few. In an overview, Figure 3.2 describes the process. Each subsection in this section provide the details.

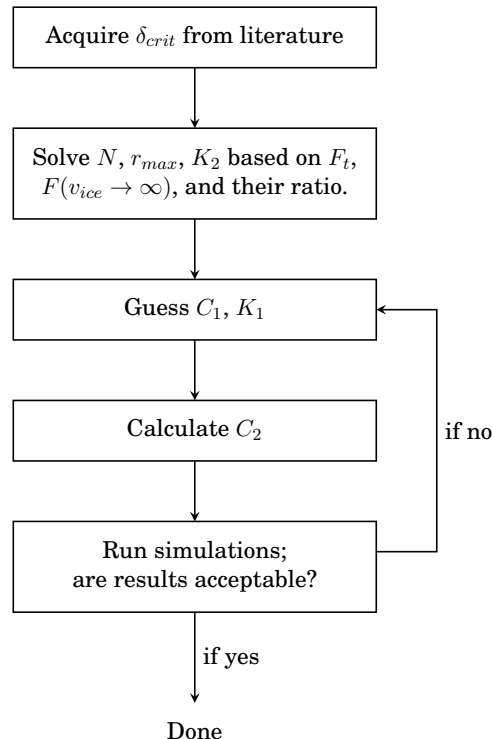


**Figure 3.2.** The data-analysis part of the calibration method has five steps. Note that the positions of  $r_{max}$  and  $\delta_{crit}$  are essentially interchangeable, where one must be taken from literature and the other fitted to measured data. Obviously, one or the other can also be measured, but this thesis provides no suggestion for how to do so.

The previously established method described in Section 3.1 differs in that  $v_t$  must also be acquired from literature, and  $C_2$  is calculated in the second step. Only  $C_1$  and  $K_1$  are part of the iterative loop. Obviously, one does not need to measure plastic relaxation data in order to apply the previous method, so the experimental routine is also different.

### 3.2.1 Determining $K_2$

$K_2$  is the spring constant of the front pure elastic component. At high ice velocities, it can be assumed that the element compression is so rapid that the dampeners have very little time to compress, i.e. the viscoelastic and creep components are almost rigid. In terms of Figure 2.10, the stress/strain relationship stays linear, leading to a quick failure. It's vital that there is no dynamic interaction, because it changes the mean load. What's more, the same high-speed CBC data is used to tune  $N$ , and dynamic interaction changes the load variance significantly.

From an analytical point of view, we can infer the mean load during high velocity CBC (The implication of CBC is that dynamic interaction effects are negligible) as product of the mean failure frequency given by Equation 3.2:

$$\text{Mean Failure Frequency} = \frac{Nv_{ice}}{0.5r_{\max} + \delta_{crit}} \quad (3.2)$$

and the mean impulse per element lifetime (as measured from spawn until failure), given by Equation 3.3:

$$\text{Mean Failure Impulse} = \frac{1}{2}K_2\delta_{crit}\frac{\delta_{crit}}{v_{ice}} \quad (3.3)$$

The product of which becomes Equation 3.4:

$$F_{mean} = \frac{NK_2\delta_{crit}^2}{r_{\max} + 2\delta_{crit}} \quad (3.4)$$

which is valid when  $v_{ice} \rightarrow \infty$ .

### 3.2.2 Determining $C_2$ by plastic relaxation tests

$C_2$  determines the rate of creep flow at any level of element load. In order to match well established research on the creep behavior of ice, the model establishes a relation between stress and plastic flow, where

$$F_{element} = \sqrt[3]{C_2 v_{creep\ flow}} \quad (3.5)$$

The standard method presented by Hendrikse [12] suggests that a series of very slow indentation tests ( $< v_t$ ) could be performed to determine  $F$  where  $v_{creep\ flow}$  is kept constant. The issue is that it is difficult to maintain a constant and very slow indentation rate, practically impossible without purpose-built machinery. Instead,  $C_2$  is usually calculated based on es-

timated  $v_t$  and  $F_t$  (as per Equation 3.1), i.e. creep is not measured directly.

In this thesis it is suggested that  $C_2$  may also be measured as a plastic relaxation experiment. The problems are that the total creep distance is extremely short, and there may not be any obvious good global reference points from which to take this measurement. To get around this, it is proposed that the ice visco-elastic component, the elastic component, as well as the elastic properties of the ram all act in series, and any drop in force over these components must correspond to a relaxation of those springs. It is assumed that after delayed-elastic response has abated, all relaxation will be due to ice creep. Thus, it's possible to calculate the velocity of ice creep if the elastic properties of the ram are measured beforehand.

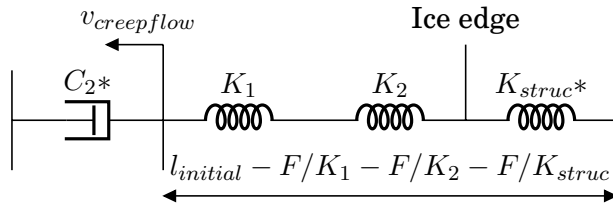


**Figure 3.3.** This figure illustrates the assumptions used to interpret the plastic relaxation tests. Note that  $l_{initial}$  is not a real distance, it merely represents a length at which all the springs are at rest.

This method allows us to measure  $C_2$ . It also allows us to measure the nonlinearity of creep. Hendrikse assumes, as shown in Equation 3.5, that the force on the element is a cube-root function of creep velocity. A new variable  $\alpha$  is introduced, replacing the 1/3 exponent to creep rate, so that Equation 3.5 becomes Equation 3.6

$$F_{element} = C_2^\alpha v_{creep flow}^\alpha \quad (3.6)$$

Where Hendrikse assumed that  $\alpha = 1/3$ . Our method of determining the nonlinearity of creep is based on requiring that  $C_2$  is a constant and we should therefore find the same value at every measurement point along the plastic relaxation timeseries. Introducing  $\alpha$  allows us to find an exponent where this requirement is met.

It's important to consider that the force acting on each ice element is not equal to the force on the ram. The force that we measure on the ram is the combined force of all elements in full synchronization. On each ice element, we have  $F$  divided by the number of total elements, i.e.  $F/N$ . The formula for solving the rate of combined relaxation of the three elastic components becomes

$$\frac{\dot{F}}{N}/K_1 + \frac{\dot{F}}{N}/K_2 + \dot{F}/K_{struc} = v_{creep\ flow} [\frac{m}{s}] \quad (3.7)$$

and  $C_2$  may be solved so that

$$\left( \frac{F}{N}/v_{creep\ flow}^\alpha \right)^{1/\alpha} = C_2 \quad (3.8)$$

The method requires picking measurement points along a plastic relaxation timeseries. In order to get good data points from which to calculate  $C_2$ , the time passed after load application must be long enough for delayed-elastic response to stop. On element level, delayed-elastic response has stopped when the springs have reached internal equilibrium.

The formula can be tested by numerically simulating a plastic relaxation test, solving  $C_2$  from that timeseries, and comparing  $C_2$  as measured to the input value. Testing shows that the accuracy of this method depends on the magnitude of  $C_1$  relative to the elastic parameters. It makes sense that treating the viscoelastic element as just a spring is only accurate when the strain rate is very low or when  $C_1$  is relatively small, because in both cases the viscous effect of the viscoelastic component can be neglected.

Another consideration is that the ram or applied structure may not have a linear elastic response. One must determine a relation between the tangential elastic modulus and the load level on the ram. An interesting observation is that compliance in the ram is not an issue for this plastic relaxation test, it actually is easier to control the applied load if there is some flexing in the ram. Compliance makes it more difficult to calibrate the other parameters.

#### *Test setup stiffness*

No structure is completely rigid, and accurately determining  $C_2$  requires a good understanding of the static stiffness of the test structure. The stiffness should be measured in relation to a global reference point, so measuring the ram from e.g. within the wagon is not acceptable. In our test, the ice was used as the static reference point. A picture of the stiffness test setup is seen in Figure 3.4.

In order to accurately determine the nonlinearity of creep, it's necessary to measure any nonlinearity in the stress/strain relationship of the rig, and an expression for the tangential stiffness modulus must be calculated.

It's vital that the load is applied without changing the stiffness characteristics of the ram, and at AIT using the wagon actuators would not have



**Figure 3.4.** A wooden beam was squeezed between the ram and the edge of the tank by extending the hydraulic cylinder in the ram.

been acceptable in this regard. Ideally, the load in the plastic relaxation test should be applied using the same mechanism as when the rig stiffness is measured.

It is also necessary to lock the position of the wagon, so that the wagon does not shift position due to the loads, which may be up to 10 kN. This was achieved by hammering wooden wedges between the bridge rail and wagon wheels.

The results of the rigidity test can be seen in Figure 3.5.

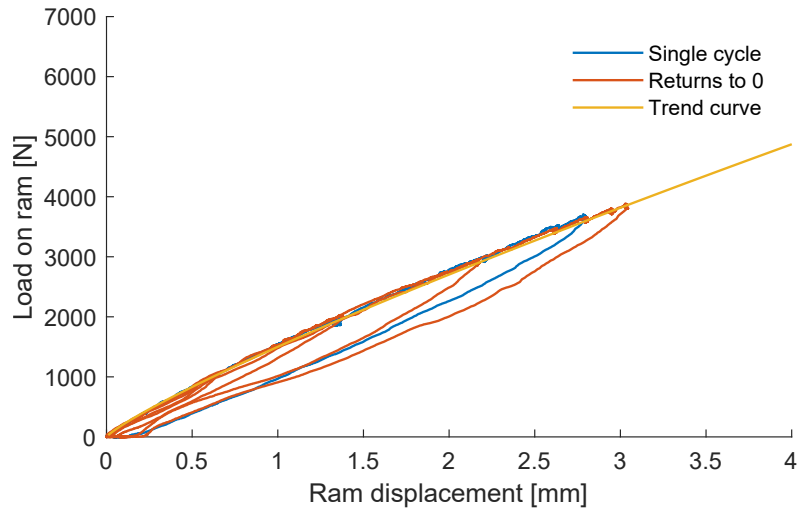


**Figure 3.5.** Two load series are included in this figure. To determine whether the wagon was slipping despite the wedges, one series cycles back to 0 displacement between load increments.

Due to the wooden beam buckling at about 4 kN, it was not possible to measure stiffness above this load.

### 3.2.3 Determining $K_1$ & $C_1$

$K_1$  and  $C_1$  are parameters that control the delayed elastic response of ice. The delayed elastic response may be seen in action in Figure 4.6. The standard way of determining them is to fit mean global loads at low speeds

(above creep transition velocity  $v_t$ ) to empirical data by manipulating  $K_1$  and  $C_1$  once  $N$ ,  $K_2$ ,  $\delta_{crit}$ ,  $r_{max}$  have been determined.

Note that even a small change in  $K_1$  requires  $C_2$  to be recalculated, a process which can be automated if one so desires.

In this thesis, the merits of determining the viscoelastic parameters based on delayed-elastic response in a plastic relaxation lab test are also evaluated. To do this,  $K_1$  and  $C_1$  are found by carefully resimulating a plastic relaxation experiment and choosing  $K_1$  and  $C_1$  such that the delayed-elastic response is as similar as possible to the delayed-elastic response seen in the plastic relaxation test. The method requires mimicking the loading pattern of the measured load timeseries, and any parameter changes may also require adjusting the loading pattern, making this method very iterative at time consuming. Also note that this method does not replace empirical data from medium-low indentor speeds, as they are needed to determine  $K_2$ ,  $N$ , and  $r_{max}$ . The results from tuning  $K_1$  and  $C_1$  to delayed-elastic response as-measured are shown in Section 4.2.1.

### 3.2.4 Determining $N$

$N$ ,  $\delta_{crit}$  and  $r_{max}$  all influence the mean failure frequency as well as the mean contact ratio (how many elements touch the structure at a point in time) in CBC. Increasing the number of elements requires a decrease in the mean impulse per element failure if the mean global ice load is to remain constant. A high frequency of weak elements failing naturally makes any element synchronization due to spawn distance randomness less likely. Thus,  $N$  is related to global ice load variance.  $N$ ,  $\delta_{crit}$  and  $r_{max}$  must all thus be chosen so that the temporal variance in global load matches an empiric CBC data source, model scale tests in our case.

### 3.2.5 Determining $r_{max}$

$r_{max}$  is the maximum distance from the structure that an element is allowed to spawn following an element failure. We have already established that  $r_{max}$  is related to mean contact ratio during CBC. The mean contact ratio is strongly related to mean global ice load. Considering that maximum global ice load requires a contact ratio at 100 %,  $r_{max}$  must be chosen so that the ratio between maximum theoretical load and mean loads during CBC is accurate to empirical measurements.

There is a clear physical interpretation to  $r_{max}$ , where it should correspond to spalling behavior, but given other simplifications that this model makes, it's unclear whether it is possible to measure  $r_{max}$  through a physical experiment such that the model preserves statistical accuracy in terms of maximum and mean global ice load.

### 3.2.6 Determining $\delta_{crit}$

$\delta_{crit}$  is the maximum allowed compression in the front pure elastic component. It should not be considered a level of compression at which the element breaks, as the viscoelastic component will also compress. At low speeds, the viscoelastic component may actually compress significantly more than the pure elastic component. Thus, the actual elastic compression is always larger than  $\delta_{crit}$  when element failure occurs. At very high ice velocities, the difference in real compression from  $\delta_{crit}$  is negligible.

Along with the stiffness parameters and  $N$ ,  $\delta_{crit}$  must be chosen so that the theoretical total load,  $F_t$ , represents a realistic value.

There isn't an obvious great way to find  $\delta_{crit}$ , other than treating it as a tool to fit the statistical means, spreads, and peaks. At the same time, the rest of the parameters can be fitted around an estimate of  $\delta_{crit}$ , so we choose to do our calibrations with a  $\delta_{crit}$  of 0.002 m, as was found in the HSVA tests [12].

### 3.2.7 Parameter fitting

It's unclear whether the BK model or the other assumptions of the model fit ice so well that it is possible to base many parameters on measurements in nature. E.g. choosing  $r_{max}$  to some mean spalling distance, and choosing  $\delta_{crit}$  to match a measured quantity creates two constraints in our calibration under which other parameters must go to extremes in order for the statistical mean behavior to match reality.

Over-constraining the calibration process is a problem, but observe that defining more parameters through physical measurements rather than using "free" parameters as curve fitting variables is useful because one may circle back to improving the accuracy of the assumptions in the base phenomenological theory.

### 3.3 Aalto Ice tank test matrix

Run Index	Run Speed [mm/s]	Run length [m]	Run time [s]	Ice field position	Target variable
11	10	1,2	120		C1 & K1
12	15	1,8	120		C1 & K1
13	20	2,4	120	Left	C1 & K1
14	25	3,0	120		C1 & K1
21	40	5,7	143		C1 & K1
22	70	10,0	143	Middle Left	C1 & K1
23	100	14,3	143		C1 & K1
31	150	12,9	86		C1 & K1
32	200	17,1	86	Middle Right	C1 & K1
41	400	13,3	33		K2
42	500	16,7	33	Right	K2

**Table 3.1.** Test matrix for the experimental model scale tests in this thesis. If a  $\delta_{crit}$  value is taken from literature, the parameters  $N$ ,  $K_2$ ,  $K_1$ ,  $C_1$  and  $r_{max}$  can be determined based on these runs. In addition, a plastic relaxation test was performed, from which  $C_2$  and  $\alpha$  are determined.

The aim of the model scale tests were to find a set of ice parameters for AIT ice. There is always some variation in the ice generated at AIT, and it is not possible to measure  $\delta_{crit}$ , so our calibration results can not be the one "true" solution, the best case is merely a set of parameters that has statistical behavior true to what was measured.  $\delta_{crit}$  could be larger or smaller, and for any one value of  $\delta_{crit}$ , there is only one set of parameters that may be found according to our strategies presented in Section 3.2.

A second objective was to test a new method for determining the parameters related to creep.

A third objective was to make quantitative observations that may be used to reiterate target ice conditions, expectations and the test matrix for the planned SHIVER test campaign.

The matrix for our tests may be seen in Table 3.1. The low end of the speed range was chosen to investigate what the lowest speeds at which the wagon can maintain reasonably constant velocity is. It's also vital to have ample data points in the lower speeds, because  $K_1$  and  $C_1$  are calibrated on the basis of low indentation-rate tests.

The high end of velocities was chosen to ensure with no uncertainty that the failure mode is CBC. These tests are allocated more ice length, so that the time series is sufficiently long. In order to investigate any possible ice load per ice speed trend, it's necessary to have several data points in CBC, which is why we chose to have two very large ice velocities at the top end.

In addition to the run shown in Table 3.1, a plastic relaxation test was performed.

### 3.3.1 Ram structure

The design goals for the ram were to reuse parts from the February pre-tests, incorporating a hydraulic cylinder for performing controlled indentation during the plastic relaxation tests, and lastly to retain enough rigidity in order to minimize structural movement due to ice load.

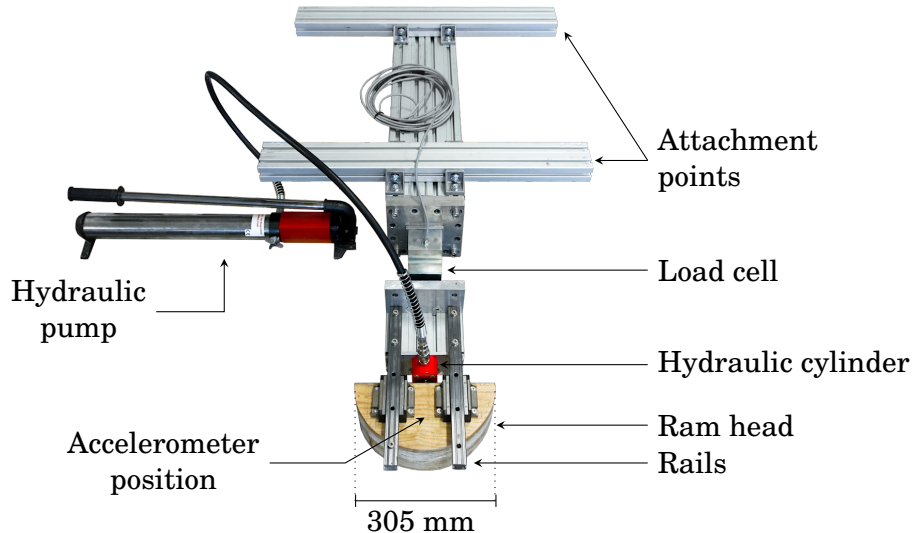


**Figure 3.6.** The general components of the ram structure are shown. A schematic drawing of the ram is found in Appendix C.

The ram support structure is built from extruded aluminum profiles, while the ram head is plywood coated with epoxy. The rails are sliding bearing systems.

A HBM 1-PW29C3/1T-1 single point load cell was used (referred to as Load cell in Figure 3.6). The load cell has favorable properties in terms of sensitivity to load misalignment, as well as low sensitivity to operating conditions. However, it is not very stiff.

For measuring vibration of the ram head, a Brüel & Kjær type 4393 accelerometer, a Brüel & Kjær signal conditioning amplifier and an Oros OR25 Model 300 DAQ were used.

The MEGANEX hydraulic cylinder was rated for 10 tons with a maximum travel of 11 mm.

### 3.4 Overview of code implementation

In order to better understand the phenomenological model, as well as to have a model that can flexibly be adapted to suit different simulation needs, a new MATLAB implementation of the model has been written during the process of this thesis.

The implementation is characterized by forward Euler timestepping with linear interpolation for sub-timestep handling of ice element failure and spawning. Euler timestepping was chosen as it reduces the need for any sub-timestep operations, as timesteps must either way be very short. However, implementing sub-timestep handling of element failures proved unavoidable in order to reach acceptable accuracy, especially considering that the short  $\delta_{crit}$  value makes individual elements touch the structure for typically very brief moments.

The element level equation of motion is solved by iterating upon a linearized solution for the creep element. A linear system of equations does not allow for an exponent to  $\dot{u}_{creep}$ , so  $\dot{u}_{creep}^{C_2 \exp -1}$  from the previous iteration is multiplied into  $C_2$ , according to Equation 3.9. This effectively linearizes the equation.

$$F_{creep} = \dot{u}_{creep}(\dot{u}_{creep,n-1}^{(\alpha-1)} C_2^\alpha) \quad (3.9)$$

This value can then be iterated upon until the linearized  $F_{creep}$  is within a specified tolerance from  $F_{creep}$  as calculated by Equation 3.10.

$$F_{creep} = \dot{u}_{creep}^\alpha C_2^\alpha \quad (3.10)$$

Thus the iteration loop can be stopped when the condition of Equation 3.11 is fulfilled.

$$\left| F_{element} - C_2^{C_2 \exp} \dot{u}_{creep}^{C_2 \exp} \right| < \text{specified tolerance} \quad (3.11)$$

The final nonlinearized values of  $C_2$  (per element per timestep) may then be recorded to be used as an initial guess for first iterations, which dramatically reduces the number of necessary subsequent iterations.

There are several additional optimizations that may be implemented, such as a more sophisticated guessing algorithm that also predicts a change in  $F_{element}$  when the effective  $C_2$  value is iterated upon, but speed has not proven to be an issue.

As  $C_2$  is typically a very large constant, so the iterative changes to  $\dot{u}_{creep}$

have an almost insignificant effect on the viscoelastic and pure-elastic components. Therefore, the tolerance can be quite lax in most applications.

One useful property of the code is the ability to run several simulations (at e.g. different constant ice velocities) in parallel, making full use of multicore CPUs as well as providing an output structure well suited for straightforward data processing.

One drawback of the implementation is that readability is poor, as using custom functions (e.g. to solve the element EOM) causes a relatively large amount of overhead.

The state of each element I have chosen to describe as a five cell vector. The values in each cell vector correspond to 1: Position of rest in global coordinate system. 2: Compression in creep component, 3: compression in viscoelastic component, 4: compression in elastic component, and finally 5: which is either 0 or 1 depending on if the element has been in contact with the structure, i.e. whether it has been activated or not. This element representation is quite useful as if the element is in contact with the structure, Equation 3.12 must be true, and this condition is used as one condition in the linear system of equations.

$$struc\_p - e_1 = -e_2 - e_3 - e_4 \quad (3.12)$$

In pseudo-code, the structure of the code can be described as in Figure 3.7.

The code has been validated by comparing results to Hendrikse's example implementation, and it performs with reasonable accuracy. In retrospect the implementation choices made by Hendrikse, especially the use of variable timestep length, I can now appreciate.

### 3.4.1 Other numerical implementations

Siemens Gamesa has coupled the model for dynamic ice interaction into their in-house software [13]. That implementation, referred to as VANILLA, coupled with BHawC, has been verified by DNV. My implementation based on the same phenomenological model, but is not VANILLA and is thus mostly referred to in my thesis as simulation model, or model for short. When I mention phenomenological model explicitly, I refer to the base theory that these implementations are built on.

```

Initialization
Set e.g. different ice velocities to be used in each run
Set different run lengths for each run if necessary
for For each run do
  for Each timestep do
    Record the positions of everything
    Activate any element that touches the structure
    for Each element do
      if Element is activated then
        Solve linear system of equations with initial guess for
        linearized  $C_2$ 
        while  $C_2$  accuracy condition not fulfilled do
          Update linearized  $C_2$ 
          Solve linear system of equations
        end
        Update element state
        if  $F_{element} > K_2 * \delta_{crit}$  then
          Do sub-timestep routine for calculating average
           $F_{element}$  in timestep
          Do sub-timestep routine for accurately respawning
          the element within  $[0, r_{max}]$  regardless of if it
          spawned early or late in the timestep
        end
      end
      Sum and record ice load
      Calculate structure response
      Update structure position
      Advance ice
    end
  end
  Run data analysis on all runs
  Aggregate and visualize information
  Provide new and improved initial guess value for linearized  $C_2$ 

```

**Figure 3.7.** This is the structure of loops used in the code with which means and variance are calculated, which is the version used during the calibration process.

## 4. Results

All tests (Indentation at 11 speeds, plastic relaxation test (repeated twice), as well as the rig rigidity tests) were all performed on the 15th of April, 2021. This section presents those results as well as some basic analysis. A summary is shown in Figure 4.1.

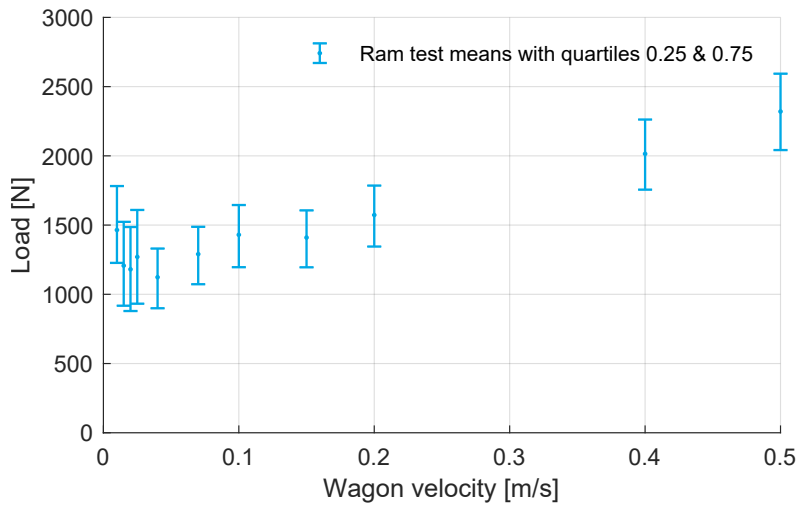


**Figure 4.1.** This figure summarizes the mean load levels of the 11 indentation runs.

### 4.1 Test data trend

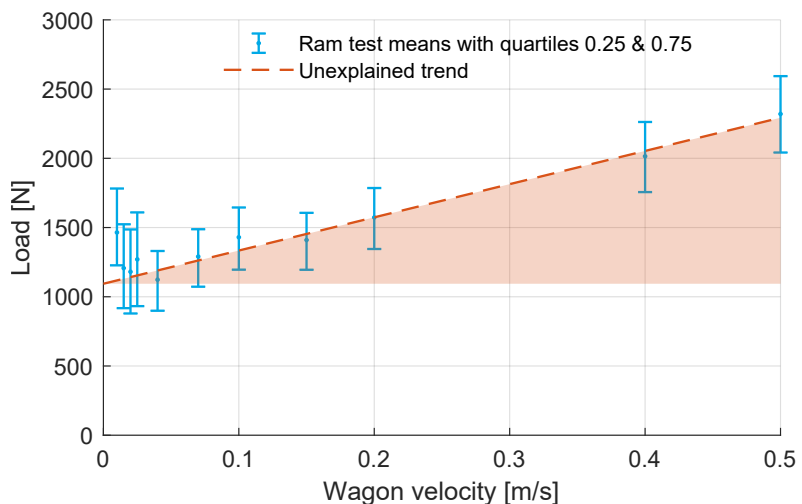


**Figure 4.2.** The unidentified speed-dependent load component has been highlighted. The trend analysis is based on a linear regression fit of the 7 highest velocity data means.

A trend where mean loads increase linearly with indenter speed is clearly identifiable among the constant speed tests, and there is no way of explaining this behavior in terms of the model. The model is designed to only predict crushing loads, so it should be expected that there is some load unaccounted for. However the strength of the trend suggests the crushing behavior was somehow fundamentally different from theory. The crushing load that can be explained by the model can only account for roughly 50% of the mean load at  $0,5\text{ ms}^{-1}$ . We may try to derive the slope of the unexplained trend, and extract the crushing load, but the physical explanation behind the strong trend is unclear, and there's no solid basis for stating that the lowest mean load measured corresponds to the CBC high speed mean load.

A more thorough analysis could be made in order to find or at least rule out possible constituents of this linear load component. Some of the unexplained force is likely made up of at least hydrodynamic drag on the ram, continuous rubble acceleration/ejection, friction between the ram and the ice, friction between rubble and ice. However it's also likely that there is something fundamentally different in the crushing failure than the type of failure that the model is designed to predict. Considering there are many other uncertainties involved, deconstructing this linear extra load component is not attempted in this thesis, and the next research focus should be on growing model ice that acts like real ice in crushing tests.

Unevenness in the strength of the ice may have also influenced the loads. Ice strength assessments according to ITTC guidelines showed quite severe compressive strength variation ( $\pm 15\%$  of the mean), as well as thickness variation in different measurement locations. However there is not enough information available to correct this after the fact. The spatial grouping of the test runs may be seen in figure 4.3, and it certainly suggests that location two might have had stronger ice than location 3, or that there was some sort of strength variation in the direction of the indentation.

Another explanation for the different load trends at location 2 and 3 could be a change in the dynamic interaction at a speed somewhere between 100 mm/s and 150 mm/s. The accelerometer data and the interquartile range of the loads however do not support this theory.

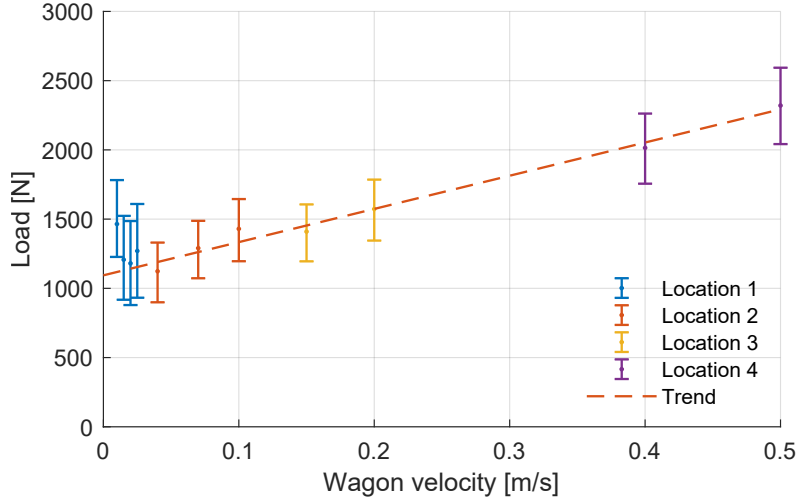


**Figure 4.3.** It appears that there is a different load trend between locations 2 and 3, indicating that there may have been a lengthwise strength or thickness gradient in the ice. The locations are 10 meters apart in width.

## 4.2 Plastic relaxation test and $C_2$

In Figure 4.4 the raw data from a plastic relaxation test is shown (one out of two plastic relaxation tests), along with  $C_2$  values solved for points where the delayed elastic response looks to have ran its course. Where the load level increases, the calculated value for  $C_2$  decreases, as indicated by the orange trend line. One must then choose whether creep behavior should be accurate at high loads or at low loads. Approximating  $C_2$  at  $0, 5 * F_t$  could be a viable strategy to get creep behavior which is most accurate most of the time, but this choice leads to an exaggerated magnitude for  $v_t$ .

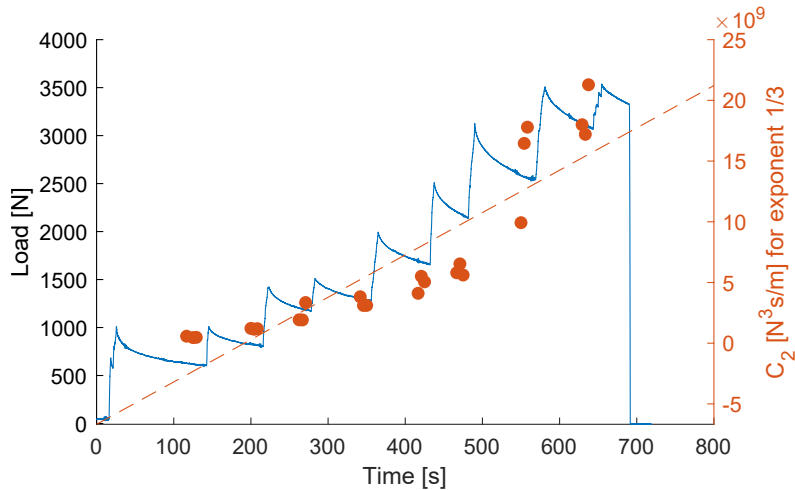


**Figure 4.4.** Values of  $C_2$  where there is a cubic relation between load and creep velocity, solved according to the method described in section 3.2.2

A cubic relation to the rate of creep flow was chosen by Hendrikse in order to better match the power law creep behavior of ice. However, fine-grained doped model ice may not have accurate creep behavior. From previous

experience, it seems that creep is very rapid in AIT ice. One may try to find a more accurate relation between ice element load and creep velocity by adjusting the exponent until the trend disappears, and we find a single value for  $C_2$  that does not depend on the load. It is shown in figure 4.5

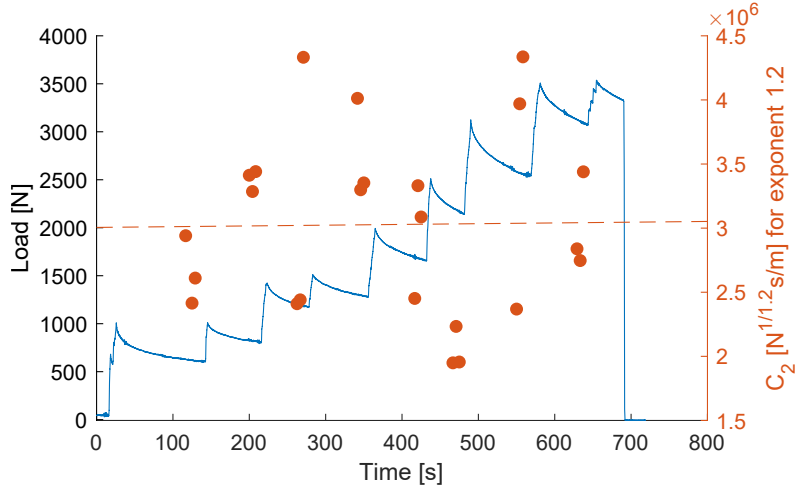


**Figure 4.5.** Values of  $C_2$  where there is a  $v_{creep}^{1.20}$  relation between creep velocity and load, solved according to the method described in section 3.2.2

A plastic relaxation timeseries was simulated using the best-fit parameters, taking into account the nonlinear compliance of the structure according to results found in Section 3.2.2. The results are shown in Figure 4.6, where the simulated plastic relaxation is showed on top of the raw plastic relaxation data. The results indicate that the methods presented in this thesis are valid for determining the creep-related inputs to the simulation. The correction to the exponent allows us to find a  $C_2$ -value where creep is more accurate at every load level measured.

Qualitatively, it may be said that delayed elastic response of the ice is also clearly seen in the plastic relaxation timeseries, which indicates that the Burger-Kelvin element model is suitable for model ice.

#### 4.2.1 Viscoelastic parameters from plastic relaxation

The results from tuning  $C_2$  from plastic relaxation are very promising, but delayed-elastic response is also seen clearly in the plastic relaxation test. It is possible to find  $C_1$  and  $K_1$  by iteratively recreating the plastic relaxation test. This process is relatively laborious, as the indentation intervals and speeds have to match that of the measured load timeseries. Using linear creep instead of an exponent of 1.2 allows for speeding up simulations. Reasonably accurate parameters for assessing the feasibility of tuning the viscoelastic parameters based on measured delayed-elastic response have

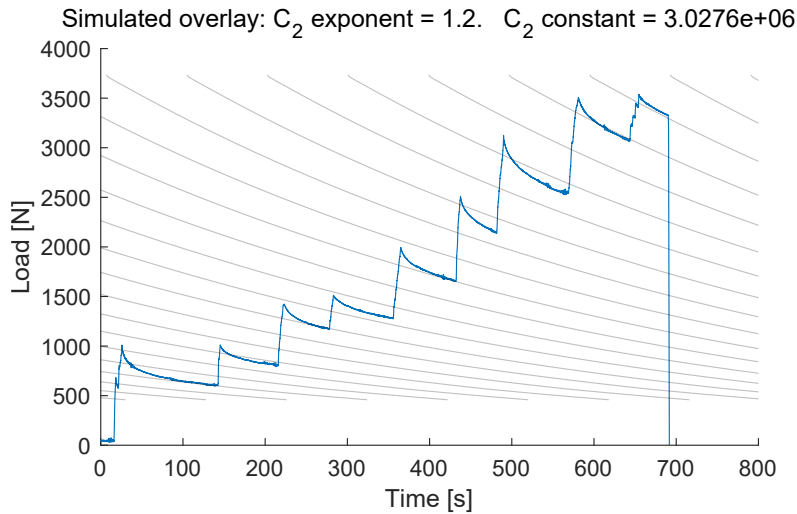


**Figure 4.6.** Plastic relaxation timeseries overlayed with a simulated plastic relaxation timeseries.

been found, and are shown in Table 4.1. The visual representation of the fitting process is shown in Figure 4.7

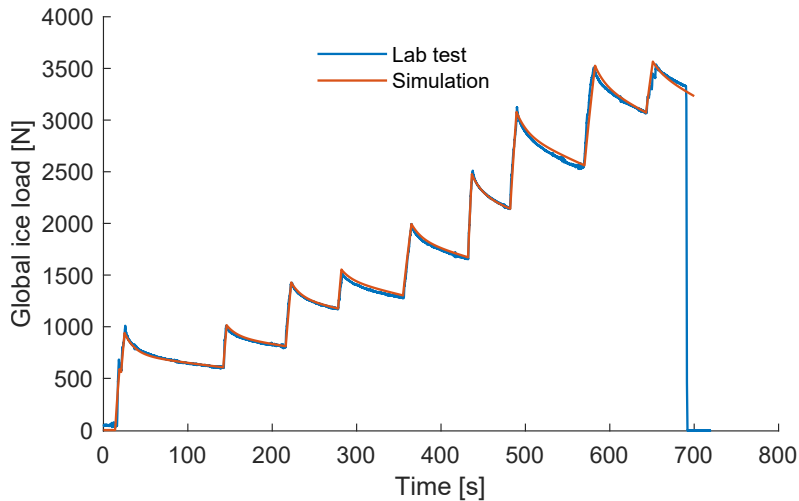


**Figure 4.7.** By tuning ice parameters and the indentation pattern, it's possible to resimulate the plastic relaxation test very well, despite the intentional "error" (Choosing a  $C_2$  exponent of 1 when 1.2 has been established to be the best fit for this load timeseries) in the creep exponent. Parameters that may not be tuned this way are  $N$ ,  $\delta_{crit}$ ,  $K_2$ , and  $r_{max}$ .

While it is possible to tune visco-elastic parameters based on the response in a plastic relaxation test, it appears to be a bad idea. Accurate delayed-elastic response is not the purpose or main priority of this phenomenological model, and any way of tuning parameters must be verified by whether they produce accurate results in the intended use case of the model. As can be seen in Figure 4.8, this tuning does not predict constant velocity indentation mean loads accurately, and is thus not a good calibration. Qualitatively it can be said that the longer timeframe and lesser magnitude of the delayed elastic response also makes especially FLI less likely to occur, as FLI requires a significant load dependency on

$K_2 =$	80000	[N/m]
$K_1 =$	$0,6K_2$	[N/m]
$C_1 =$	839520	[Ns/m]
$C_2 =$	8,69E+06	[Ns/m]
$N =$	55	[ $\cdot$ ]
$r_{max} =$	0,012	[m]
$\delta_{crit} =$	0,002	[m]

**Table 4.1.** This table summarizes the parameter choices found by calibrating viscoelastic parameters for plastic relaxation. Note that the value of  $C_2$  is tuned for linear creep behavior, and as seen in Figure 4.7, this is not a good set of parameters.

whether the structure is in phase vs out of phase with ice movement.

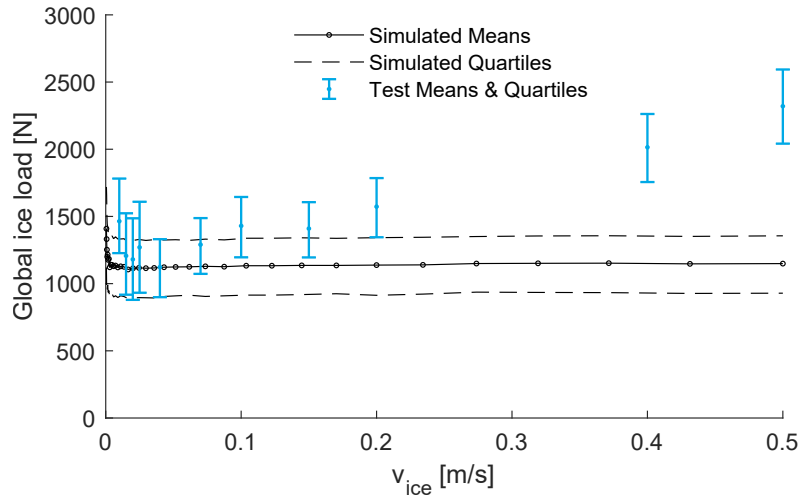


**Figure 4.8.** Fitting  $C_1$  and  $K_1$  based on delayed elastic response as measured in a plastic relaxation tests yields unsatisfactory predictions for means loads at low speeds.

The stiffness  $K_1$  of the visco-elastic component is much larger when it is based on measured delayed elastic response when compared to how it's normally calibrated. The strain-rate dependent strength of ice must thus be misrepresented in order for the phenomenological to be statistically accurate at low speeds. This indicates that there is something missing on the phenomenological level.

The relative weakness of the delayed-elastic response (a high  $K_1$ ) is a result that looks similar to Sinha's [14] experiments on delayed-elastic strain, however his results seem to indicate that not only delayed-elastic response is recoverable, but that there is some recoverability in creep as well, which is difficult to reconcile with our results. It seems like his interpretation of what is creep and what is delayed-elastic response is different from our assumptions and how the Burger-Kelvin element works.

### 4.3 Ice-structure interaction analysis

This section provides some basic qualitative and quantitative analysis of the ice-structure interaction which provides useful signals on whether the ice was acting according to theory or not. No structure is completely rigid, so the data must be analyzed to see whether or not interaction effects are significant.

Significant ice-structure interactions (Where the movements of the structure affect the ice) cause an increase in the mean load on the structure in addition to creating a periodic load variation around the mean, depending on the phase of the structure movement. Calibration is simpler if structural variables may be eliminated via assuming that the structure is rigid enough that little interaction occurs, however this must be validated.

#### 4.3.1 Identifying intermittent crushing

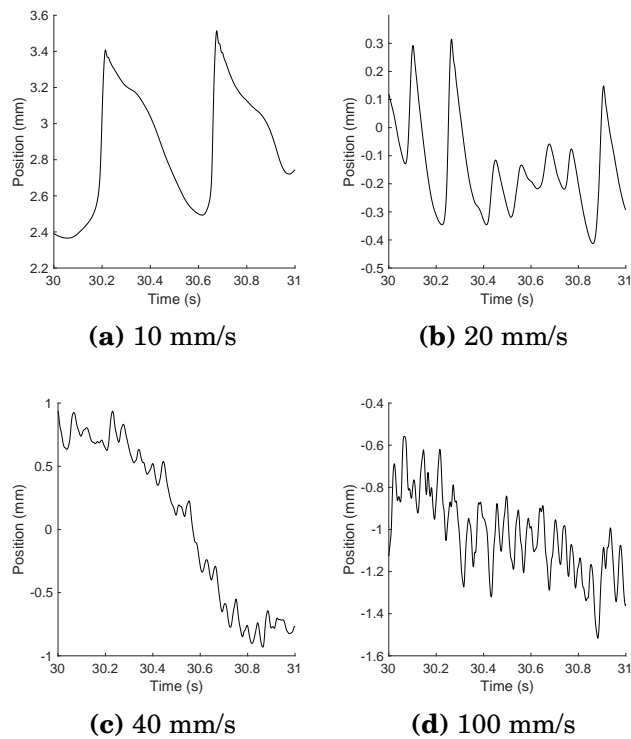


**Figure 4.9.** This figure shows the ram position history relative to the wagon position during crushing runs. Note that the choice of coordinate system is consistent with previous figures, where the ice comes from the positive y-direction. In plots a) and b), the pattern is typical for IC failure regime, based on theory presented in Section 2.1.

The ram was fitted with an accelerometer that recorded linear acceleration in the direction of wagon travel. The data has been cropped so that wagon acceleration and deceleration is not included. Thus, the mean velocity during the data window should be roughly equal to zero, as the wagon

moves with a near constant velocity. With this treatment of the velocity as integrated from the accelerometer timeseries, we may integrate and receive the position of the ram relative to the wagon. The integration constant used when integrating velocity into position is of little relevance is chosen to be 0.

The resulting information about the vibration of the structure is shown in Figure 4.9, and IC may be clearly identified through the displacement pattern. The findings agree with a qualitative assessment from video footage of the tests, where a thudding sound is released with approximately equal intervals as between IC failures. At 20 mm/s, one can hear clear intermittency. Beginning at 100 mm/s, the noise can be described as an even scraping sound, with no hints of any intermittency.

### 4.3.2 Identifying resonant lock-in

Due to the relative lightness of the ram structure, the ram's stiffness, the low loads, and damping from being submersed in the water, the necessary conditions for FLI should not occur.

During pre-tests in February 2020 at AIT, the same ram structure did see FLI for brief moments at a wagon velocity of 100 mm/s, however the excited frequency seemed to be an eigenfrequency of the wagon, not of the ram, which is attached firmly to the wagon. The same behavior was not seen in our tests, where the loads were weaker and the excitation is less likely to overcome damping, and thus steady FLI is unlikely.

The analysis is further confused by the fact that several eigenfrequencies are somewhat excited, but none is dominant in our tests.

The relationship between ice velocity and FLI structural vibrations as described in Section 2.2.1 states that the maximum cyclical structural velocity should be near or above ice velocity during FLI. A 99th quantile calculation of the absolute structural velocity timeseries at each run speed indicates that structural velocities did not reach wagon velocity during our tests, except for in tests where there is clear IC.

### 4.3.3 Modal analysis of ice-structure interaction

A couple conclusions may be drawn from Figure 4.10, which presents an FFT-analysis of a couple runs. The mean absolute velocity seems to be increasing with indentation speed, and it clearly shows that the excitation happens in two modes at high velocities. This indicates that a 1

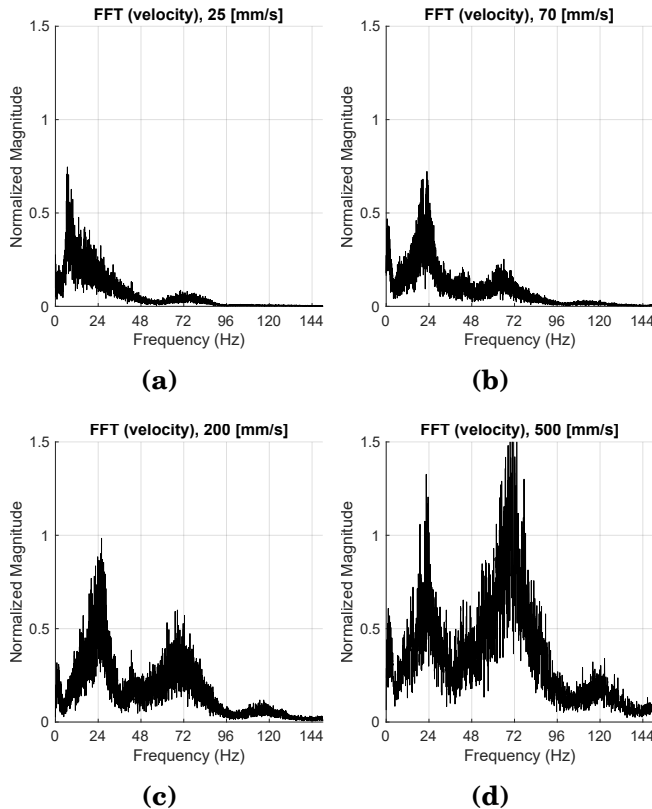


**Figure 4.10.** The FFT-decomposition of the velocity timeseries for each run reveals two structural eigenfrequencies with significant excitation.

DOF structure representation can not be sufficient to resimulate the high velocity runs. An advanced structural analysis to determine the coefficients for accurately describing a two or three DOF structure representation is not within reach in the timeframe of this thesis. However preliminary results from simulating a 2 DOF oscillator with eigenmodes at 24 and 64 Hz indicate that the interaction effect is not strong enough to significantly throw off calibration results.

#### 4.3.4 Buckling and its effects

Buckling is an unwanted phenomenon when we are trying to test crushing against a vertical structure. In the worst case, it may make calibration data unusable. As AIT model ice has a strong strength gradient, where the bottom of the ice is especially mushy, there were concerns that buckling may be an issue.

During a plastic relaxation test, buckling may cause loads to dissipate faster than expected. In our tests, buckling was not a problem. No attempt to accurately quantify buckling was made, but by placing a straight-edge on the ice it was approximated that the downward ice displacement in the vicinity of the ram was less than 2 mm. The geometry of our ram makes it

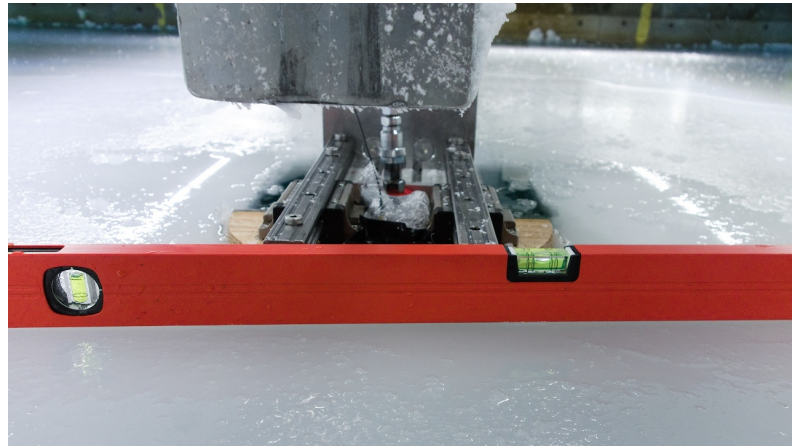


**Figure 4.11.** No significant buckling occurred during the plastic relaxation tests. A straight-edge was used to assess any curvature in the ice.

prone to bending downwards under a load at the ram head, which could influence buckling of the ice sheet.

During the tests at speed, no indication of buckling failure was identified.

#### 4.4 Parameter results

By detracting the trend (Discussed in Section 4.1), it is possible to find parameters that reproduce the detrended crushing loads. The parameters are shown in Table 4.2, while the fit is shown in Figure 4.12.

$K_2 =$	72000	[N/m]
$K_1 =$	$0,2K_2$	[N/m]
$C_1 =$	$0,413K_2$	[Ns/m]
$C_2 =$	$5.259\text{e+06}$	[Ns/m]
$N =$	55	[ $\cdot$ ]
$r_{max} =$	0,012	[m]
$\delta_{crit} =$	0,002	[m]

**Table 4.2.** This table summarizes the ice parameters used to generate Figure 4.12. Note that the value of  $C_2$  is tuned for linear creep behavior. The parameters are a reasonably good fit to the experimental data and correspond to the reference ice conditions presented in Table 4.3.

However, the calibration is not particularly useful as we can't explain the trend, and we can't verify that the same factors that cause the trend do not also cause premature ice failure at low speeds, causing weak mean loads. Calibration parameters from further testing in the SHIVER campaign may shed light on the subject.

The basic ice properties of the model ice used in our tests was measured according to ITTC guidelines, and are presented in Table 4.3. In order to achieve conditions where we expected ideal crushing behavior, the ice was not tempered.

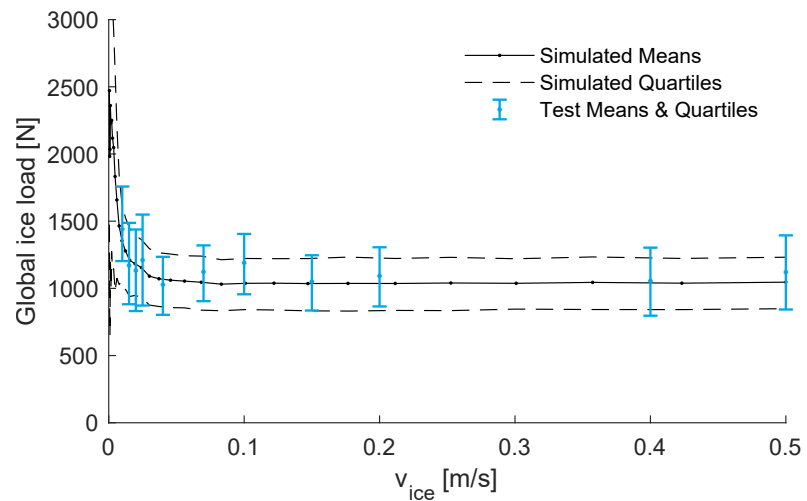


**Figure 4.12.** The parameters presented in Table 4.2 accurately reproduce mean loads in general, but fail to capture the variance at the lowest and highest speeds.

$\sigma_{compressive}$ (Mean) =	286 kPa
$\sigma_{compressive}$ (Std. dev) =	54 kPa
$\sigma_{flexural}$ (Mean) =	154 kPa
$\sigma_{flexural}$ (Std. dev) =	6,7 kPa
$h_{ice}$ (max) =	56 mm
$h_{ice}$ (min) =	42 mm
$E$ (Strain Modulus) =	434,5 MPa

**Table 4.3.** The ice conditions shown in this table were measured prior to testing.

## 5. Discussion

This chapter provides further context, suggestions and comments on the methods used and the resulting parameters.

Suggestions for further research can be found in Sections 5.3, 5.2.4, and 5.2.3.

### 5.1 Comparison to pre-tests

Similar tests at AIT were done in February of 2020. Some of the same structure parts were used, and the size of the structure was the same. A comparison between the results of our tests and the pre-tests is shown in Figure 5.1. Note that the pre-tests saw higher loads, despite their ice having far lesser compressive strength. The ITTC compressive strength assessment appears to have been done differently between the two tests. There have been modifications to the testing apparatus since February 2020, which may explain why the compressive strength seems low for the pre-test. The apparatus has been made more stiff to reduce bending, and a silicone pad has been added, which helps to prevent premature compressive failure of the ice due to uneven contact.

The ice generation process was also different during the pre-test. The ice had gone through the normal generation process of spraying, freezing and tempering, then some tests were done, after which freezing was restarted. After the second round of freezing, the ice was dramatically hardened. It's possible that the ice was cooler than usual during the pre-test, as tests proceeded right after the freezing stage. Ice temperature may affect the failure behavior of ice. The ice surface temperature was not measured during my test, but it's likely to have been near 0 degrees Celsius.

The pre-test ice performed as intended, and our test did not. We had thought that it was key to have as hard ice as possible to get the right ice behavior, but it turns out there is something else influencing the failure behavior.

The details of the ice conditions during the pre-test are shown in Table

## 5.1.

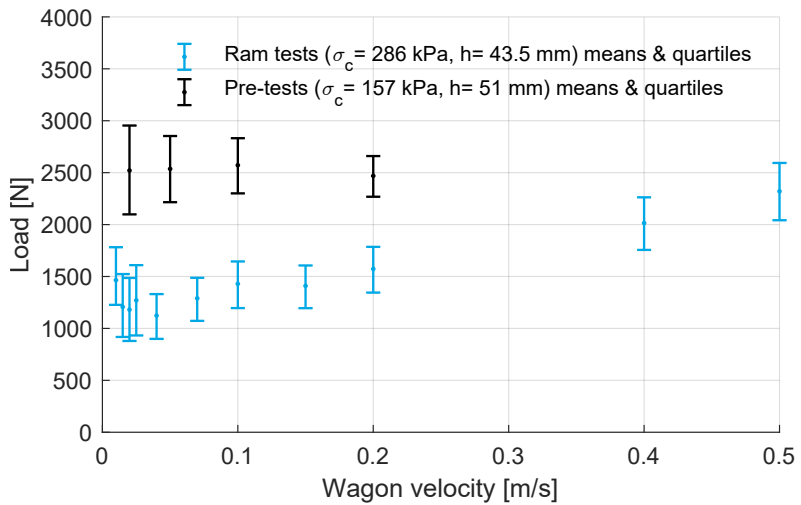


**Figure 5.1.** The context of earlier tests performed at AIT put the validity of our results into question, as the cause behind the significantly different behavior is unknown.

$$\begin{aligned}
 \sigma_{compressive} &= 157 \text{ kPa} \\
 \sigma_{flexural} &= \text{Not measured} \\
 h_{ice} &= 51 \text{ mm} \\
 E \text{ (Strain Modulus)} &= \text{Not measured}
 \end{aligned}$$

**Table 5.1.** During the pre-tests at AIT in February of 2020, the following ice conditions were reported.

In all tests, the same plywood half-cylinder with a diameter of 305 mm was used. However, due to the addition of the hydraulic member in our tests, the structure was less rigid, and prone to vertical movement due to the load cell support and load application misalignment. There was little or no vertical movement of the ram during the pre-tests, as there was less horizontal distance between the ram head and the load cell support. This is one possible partial cause for the diminished loads, and could be verified with another round of testing.



(a) Pre-test at 20 mm/s

(b) Test at 20 mm/s

**Figure 5.2.** A visual comparison of the test and pre-test.

In Figure 5.2 it's clearly seen that the size of the generated ice chunks was far finer in the pre-tests. This is contrary to what was expected, as

the ice field with the greatest compressive strength also generated the finest chunks during the pre-tests. Another qualitative observation is that long cracks in the direction of the travel were created in the ice during the pre-test, which did not occur at any speed during our tests. Significant steady vibrations at around 1 Hz were also observed during the pre-test at 100 mm/s in the hard ice. The global ice load was almost twice as high as during our test at that velocity.

In light of what's presented in this section, it is not yet clear how to create model ice at AIT that behaves as expected in crushing against a vertical structure.

## 5.2 Plastic relaxation tests in model ice

The plastic relaxation tests for determining  $C_2$  and the nonlinearity of the creep behavior has proven to be a straightforward method that results in clear and easily-interpreted data. The same data is not suitable for calibrating the delayed-elastic response, not within the framework of the current phenomenological model. This section provides additional context to the method.

### 5.2.1 Method for determining $F_t$

Hendrikse calibrates the model according to an assumption that 100% of the number of elements in the simulation only correspond to a real contact area of 1/3 of the nominal contact area (Personal communication, Hayo Hendrikse 3.6.2021). This assumption makes it difficult to do plastic relaxation tests, as it is necessary to know how much area is in contact with the structure during the plastic relaxation test. Perhaps one could use three times the total number of elements for the  $C_2$  calculation.

However the model has contact area variation built in, and the assumption that  $N$  elements only correspond to 1/3 of the nominal contact area may be redundant. The assumption also leads to an  $F_t$ , which is the maximum ice load that the model can reproduce, that doesn't correspond to the maximum load the ice may inflict. The  $F_t$  used in this thesis corresponds to the maximum load measured during the plastic relaxation test, i.e. a contact area close to the nominal contact area.

These factors are what lead to a lower apparent ratio of  $F_{mean}/F_t$  than what has previously been reported, as well as the high  $r_{max}$ , which facili-

tates the low average contact ratio, as well as a high  $N$ , which keeps load variance low when the increased  $r_{max}$  had the opposite effect.

Given that we also determine  $F_t$  in a slightly different manner than Hendrikse, which is mentioned in greater detail in Section 5.2.1, there is one other parameter solution. In this other solution,  $r_{max}$  is significantly smaller, and elements are fewer in number.

Note that we didn't have the correct failure behavior in our ice, leading to the trend discussed in Section 4.1, which may be due to several reasons, but this is a separate issue. The discussion in this subsection has to do with calibration methodology regardless of whether the ice is acting in line with theory or not.

### 5.2.2 Practicality of plastic relaxation tests

The method applied in this thesis has three major considerations in terms of ease of employment:

It does not require a wagon or structure apparatus that is capable of maintaining constant velocities at near transition velocity. At AIT, the wagon can not maintain velocities at under 10 mm/s. The problem is further complicated by the fact that the largest loads will be measured at or near transition velocity.

An estimate for the real transition velocity may be found by applying the parameters on element level according to Equation 5.1:

$$\begin{aligned} F_t &= F_{creep}(\dot{u}_{creep} = v_t) \\ \delta_{crit} K_2 &= C_2^{1,2} v_t^{1,2} \\ v_t &= \left( \frac{\delta_{crit} K_2}{C_2^{1,2}} \right)^{1/1,2} \\ v_t &= 0,0208 \text{ mms}^{-1} \end{aligned} \tag{5.1}$$

The second consideration is that the ram has to facilitate enough indentation into the ice to reach  $F_t$ . If there is a lot of flexibility in the test structure support, some travel is lost. In our case, where the rigidity of the structure can be seen in Figure 3.5, roughly half of the hydraulic cylinder travel of 11 mm is lost in displacement of the support structure at 7 kN. This facilitation of movement should also not change the rigidity of the structure, so using electric motors might not be feasible. This may be further tested during the SHIVER campaign. It should be noted that the added length from the hydraulic member and the rails may have affected the crushing loads. The third major consideration is that the rigidity of

the structure with regard to a global frame of reference must be quantified. This may pose practical challenges. One such challenge during our tests was that the wooden post used as a support (between the ram head and the concrete basin edge) would buckle at about 4 kN, restricting us from measuring the stiffness properties of the ram above that load level. Nonlinearity of the force/displacement relationship of the ram needs to be accounted for. Failure to account for the slight nonlinearity shown in Figure 3.5 would lead to overestimating  $C_2, exp$  by 8% (1,3 vs 1,2).

Another minor consideration is that the wagon needs to be locked in place during both rigidity assessment as well as during the plastic relaxation test. At AIT there is no proper mechanism for locking the position of the wagon on the bridge, and locking was facilitated by striking wooden wedges between the wagon wheels and the bridge rail.

### 5.2.3 Accuracy & Uncertainty

The simple analytical formulas used rely on an assumption stating that creep is only occurring in the ice. In reality, there may be parasitic force losses which would lead to underestimating  $C_2$  if unaccounted for. It was our experience during the rigidity tests that the first time the load was applied, some quite significant parasitic losses were seen, which may be attributed to the wagon sliding towards the wedges, but that the parasitic loss was much reduced once the slack had been eliminated.

Accounting for parasitic losses should be possible, especially if they can be measured during the rigidity testing, but this requires understanding of exactly which part of the system the parasitic load drop comes from. More work should be done to determine the best method for taking into account parasitic losses.

The simple equations involved in calculating  $C_2$  based on a plastic relaxation timeseries make for easily interpreted data. However, as the method relies on measuring the relatively low rate of force dissipation, it is sensitive to noisy data. For example vibrations may cause enormous errors in  $C_2$  if  $dF/dt$  is measured from an oscillating signal. Depending on the quality of the data, one may have to apply smoothing or measure  $dF/dt$  over a longer timespan in order to avoid extreme  $C_2$  results.

One must be careful not to measure  $dF/dt$  in an interval where delayed elastic response dominates the rate of force dissipation. This can be ensured by waiting an appropriate duration of time between applying load and taking the measurement.

### 5.2.4 Applicability

The method for determining  $C_2$  is applicable without modification. The method is recommendable because it allows tuning  $C_2$  based on actual measurements rather than inference from findings about creep transition velocity in literature. Similar plastic relaxation tests should be performed in sea ice, to attempt to study the nonlinearity of creep.

There is an unexplored question in how the shape of the indenter may affect results. It's likely that it may affect the size of  $C_2$ , if it is assumed that the general direction of creep flow is parallel to the normal of the contact surface.

In the future, it would be useful to load the ice until failure during the plastic relaxation test. This provides a good estimate of  $F_t$  and increases the usefulness of a plastic relaxation test.

It may also be possible to estimate  $\delta_{crit}$  based on total creep distance. This has not been attempted in this thesis. At this point, there is no strategy available for validating such an estimate. Basing too much of the calibration methodology on a single data source also makes the end result sensitive errors in that data source. The applicability of this method needs to be further studied.

If further research could establish an element model or changes to the phenomenological theory which would increase the model accuracy so that delayed elastic response could be used to directly determine  $K_1$  and  $C_1$ , this would be a significant step towards the theoretical completeness of the phenomenological model. It could also provide a less work-intensive way for determining the visco-elastic ice parameters. The plastic relaxation test does not consume much ice area in the basin, and determining more parameters based on it would free up the rest of the ice for different testing purposes. Currently, tuning viscoelastic parameters based on plastic relaxation is not applicable.

## 5.3 Calibration results

The trend seen in our results was not present in the pre-test results. This suggests that the unexplained trend stems from a change in failure behavior, due to some difference in either the structure or in the ice. The failure behavior is not bending, that much is clear. The slight downward rotation of the ram head due to ice load may have induced complicated stress-

states in the ice, leading to more aggressive local ice cracking, reducing the true contact area between the ice and the ram.

In light of this uncertainty, the calibration results are unusable. More testing needs to be done in order to determine the cause of the weak failure. The hydraulic member and rails should be removed to ensure that the vertical movement is not a factor.

If the structural modifications are found not to be the cause of the changed failure behavior, failure under different ice conditions should be further explored. The pre-tests consisted of tests in hard as well as soft model ice, and the conclusions drawn from those tests state that the crushing load means have a positive trend for weak ice ( $\sigma_{compressive}$  ca. 50 kPa), but not for hard ice ( $\sigma_{compressive}$  ca. 150 kPa). Our ice was stronger in terms of compressive strength than the hard model ice used in the pre-tests, and this fact makes it difficult to form a hypothesis for the influence of ice strength on the failure mode.

### **5.3.1 SHIVER tests**

SHIVER tests are still ongoing, and will hopefully establish an ice generation process that leads to model ice with proper crushing behavior. One explanation for the unexpected load trend may be that the ice had a high content of unfrozen water. This water is expelled from the ice during crushing, resisting compression and compromising the strength of the ice. The issue can be resolved by testing at lower temperatures.

## 6. Conclusions

Due to the model ice not behaving like natural ice in crushing, it was not possible to arrive at a set of parameters which accurately reproduce the experimentally measured loads.

A new method for determining the creep-related parameters has been tested, and results are promising. The results indicate that the assumed relation between ice load and creep speed in the model, previously established as  $F_{element} = \dot{u}_{creep}^{1/3} C_2^{1/3}$ , is wrong for fine-grained ethanol-doped model ice. The practical implications of this may be that the model can be simplified, computational burden decreased, and that accuracy at low indentation speeds can be improved. The methods applied may be adapted to measuring the creep behavior of sea ice.

Results also show that measuring the real delayed-elastic response in ice is not a viable data source for calibrating the parameters governing delayed-elastic response in the model, as this does not yield accurate constant low-velocity force means. This result shall be treated with some scepticism as there were uncertainties related to the crushing loads measured in our tests, however the test could easily be repeated if an ice generation process that yields better ice is found at AIT. The implication is that there may be an ice element model that is more accurate than the current Burger-Kelvin element model.

The result of further testing in the SHIVER-campaigns at the ice tank is that ice behavior is more in line with theory when the model ice is cooled to below 15 degrees C. The mechanisms governing the change in failure behavior are unclear.

# Acknowledgements

This is a thesis that touches on many subjects, and it wouldn't have been possible to do without the assistance of some key people.

Big thanks to the boys at AIT, Otto Puolakka, Teemu Päivärinta and Lasse Turja for providing the opportunity to do model scale testing. Your help with constructing the testing equipment and your expertise in model scale ice was extremely helpful.

I also want to thank Pauli Lehto for making your insight in vibration analysis available, we garnered much additional information from the model tests thanks to your help.

I want to thank the NTNU FATICE research group where I had the opportunity to present my work to an interested audience every week, this dialogue was a boost in motivation much needed in these remote-office days. I want to thank my supervisor Knut and the NMCCE-programme for connecting me to this highly interesting topic, I have a strong feeling I wouldn't have had this opportunity if not for you!

Big thanks to Hayo Hendrikse for answering my questions when I got stuck, letting me come check out ELSA and including me in the wider context of the research.

# Bibliography

- [1] Garry Timco and B. Wright. Multi-year ice loads on the molikpaq: May 12, 1986 event. 01 2005.
- [2] L Fransson. Some observations of continuous and intermittent crushing failure of ice. *Proceedings of the 16th International Conference on Port and Ocean Engineering under Arctic Conditions, Volume 1*, pages 393–402, 2001.
- [3] Torodd S. Nord, Ilija Samardžija, Hayo Hendrikse, Morten Bjerkås, Knut V. Høyland, and Hongtao Li. Ice-induced vibrations of the norströmsgrund lighthouse. *Cold Regions Science and Technology*, 155:237–251, 2018. doi: <https://doi.org/10.1016/j.coldregions.2018.08.005>.
- [4] Hayo Hendrikse and Andrei Metrikine. Interpretation and prediction of ice induced vibrations based on contact area variation. *International Journal of Solids and Structures*, 75-76:336–348, 2015. doi:<https://doi.org/10.1016/j.ijsolstr.2015.08.023>.
- [5] International Organization for Standardization. Iso 19906:2019 petroleum and natural gas industries — arctic offshore structures, 2019.
- [6] Y Toyama, T Sensu, M Minani, and N Yashima. Model tests on ice-induced self-excited vibration of cylindrical structures. *Proceedings of the Seventh International Conference on Port and Ocean Engineering under Arctic Conditions, Volume 2*, pages 834–844, 1983.
- [7] M Määttänen. Stability of self-excited ice-induced structural vibrations. *Proceedings of the Fourth International Conference on Port and Ocean Engineering under Arctic Conditions, Volume 2*, pages 684–, 1977.
- [8] Erland Schulson. Brittle failure of ice. *Engineering Fracture Mechanics*, 51:1839–1887, 12 2001. doi:[10.1016/S0013-7944\(01\)00037-6](https://doi.org/10.1016/S0013-7944(01)00037-6).
- [9] Devinder S. Sodhi, Takahiro Takeuchi, Naoki Nakazawa, Satoshi Akagawa, and Hiroshi Saeki. Medium-scale indentation tests on sea ice at various speeds. *Cold Regions Science and Technology*, 28(3):161–182, 1998. doi: [https://doi.org/10.1016/S0165-232X\(98\)00017-2](https://doi.org/10.1016/S0165-232X(98)00017-2).
- [10] Hayo Hendrikse and Torodd S. Nord. Dynamic response of an offshore structure interacting with an ice floe failing in crushing. *Marine Structures*, 65:271–290, 2019. doi:<https://doi.org/10.1016/j.marstruc.2019.01.012>.
- [11] H. Hendrikse, G. Ziemer, and C.C. Owen. Experimental validation of a model for prediction of dynamic ice-structure interaction. *Cold Regions Science and Technology*, 151:345–358, 2018. doi:<https://doi.org/10.1016/j.coldregions.2018.04.003>.

- [12] Hayo Hendrikse and Andrei Metrikine. Ice-induced vibrations and ice buckling. *Cold Regions Science and Technology*, 131:129–141, 2016. doi: <https://doi.org/10.1016/j.coldregions.2016.09.009>.
- [13] Tom Willems and Hayo Hendrikse. Coupled simulation of ice-structure interaction of offshore wind turbines in bhawc using vanilla. 06 2019.
- [14] Nirmal Kumar Sinha. Rheology of columnar-grained ice. *Experimental Mechanics*, 18(12):464–470, 1978.

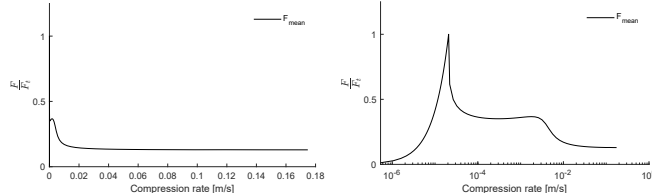
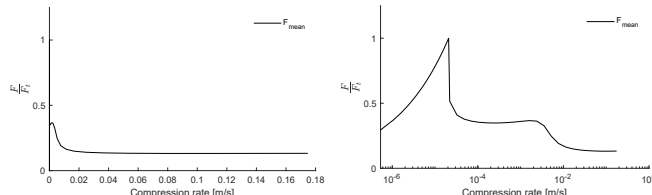
## A. Load means vs. a rigid structure based on single element response

Simulating crushing loads at a range of speeds for a set of input parameters where the number of elements is large and the creep behavior is nonlinear is computationally demanding. This type of simulation must be performed repeatedly while determining  $K_1$  and  $C_1$  through iteration. It is especially demanding at velocities near transition speed, for a number of reasons:

- Elements spend a larger portion of their lifetimes in contact with the structure, and thus require a larger number of mathematical operations.
- At just above transition speed, the elements fail infrequently. If the elements undergo only few load cycles, the simulation becomes prone to error from including incomplete cycles, which throws off the results.
- For my code, which relies on an initial guess to solve the nonlinear creep behavior at reasonable speed, no single initial guess value will work well for both velocities near transition speed and far from transition speed.

An alternative way of calculating the global mean is to simulate a single element lifetime (from spawn at  $0.5 * r_{max}$  to failure) and to infer the global load from that single element response. The mean force during the element lifetime multiplied by the number of total elements gives the mean global load. This way, for each speed increment, only one element needs to be simulated and for only one load cycle. Care should be taken to not run this calculation at any speeds lesser than  $v_t$ , as elements will never fail. The mean load at velocities between zero and  $v_t$  can be described analytically. Note that this method is only applicable to a rigid structure.

This mean trend behavior shown in Figure 1.1 is quite different from Figure 1.2, and has an unexpected positive slope at a velocity greater than  $v_t$  ( $v_t$  is at the load peak.). In Figure 1.3 where time-normalized single element failures at four speeds are shown, the reason for this hump can be seen. As the indentation rate is reduced between curves 2 to 3, the magnitude of the delayed-elastic effect is also dramatically reduced and the response is almost linear from contact to failure. In curve four at

(a)  $C_2 \text{exp} = 1.2$ , lin x-axis (b)  $C_2 \text{exp} = 1.2$ , log x-axis(c)  $C_2 \text{exp} = 1/3$ , lin x-axis (d)  $C_2 \text{exp} = 1/3$ , log x-axis

**Figure 1.1.** It appears that the choice of creep behavior has very little effect on means just above  $v_t$ .  $C_2$  was chosen so that  $v_t$  wouldn't change when the creep exponent was modified. The creep exponent has a strong effect on  $v_t$ . The other input parameters were not modified and correspond to 4.2, except for  $C_2$  and creep exponent (and  $v_t$  by extension).

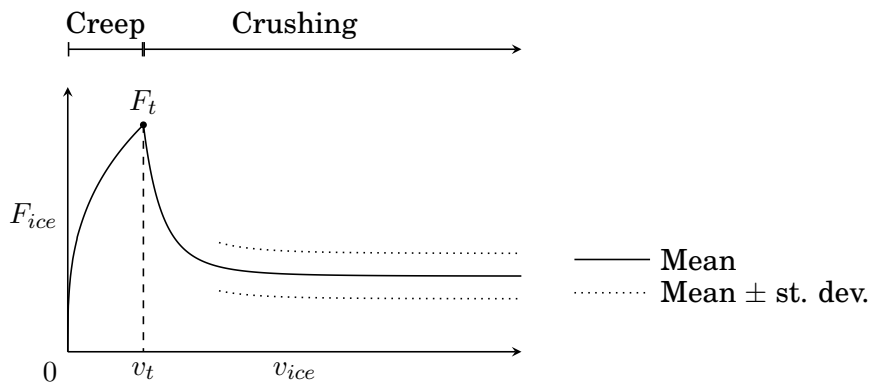


**Figure 1.2.** This is the typical curve that has been used to describe the mean as a function of  $v_{ice}$ .

$v_{ice} = 0.00003$ , delayed-elastic response has no effect on the path from contact to failure, and all of the curvature comes from creep effects.

The second effect that drives up mean global loads at near (but above)  $v_t$  is that the duration of time the element stays in contact with the structure grows faster than the duration of time it spends moving towards the structure when velocity decreases. This influences the mean failure frequency but not the impulse from a single element failure.

If the input parameters found in the thesis are combined with the model test results as seen in Figure 1.4, it's seen that the rise in mean loads at low speeds is entirely due to delayed-elastic response, and almost not affected by creep at all.  $v_t$  is far, far lower than what has been assumed in previous reference calibration attempts. The difference in principle between our value and previous  $v_t$  values is that our  $v_t$  is calculated based on  $C_2$  as measured through the plastic relaxation test, while previously

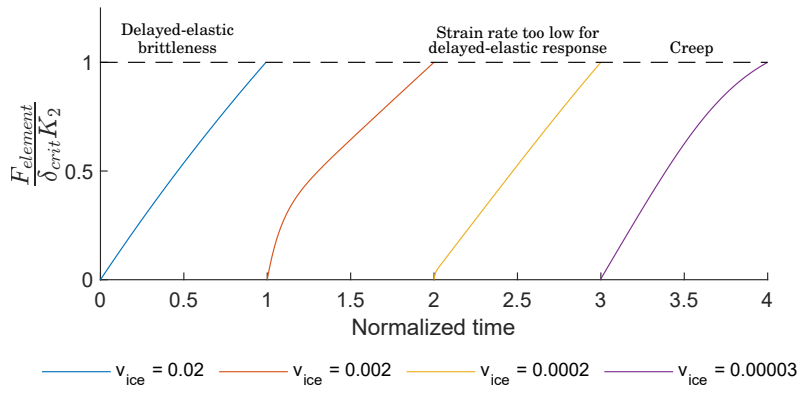


**Figure 1.3.** Time has been normalized so that it should be evident that the mean force over the duration of each contact event is higher for speeds 2 and 4 than for speed 3. This is the reason for the hump.

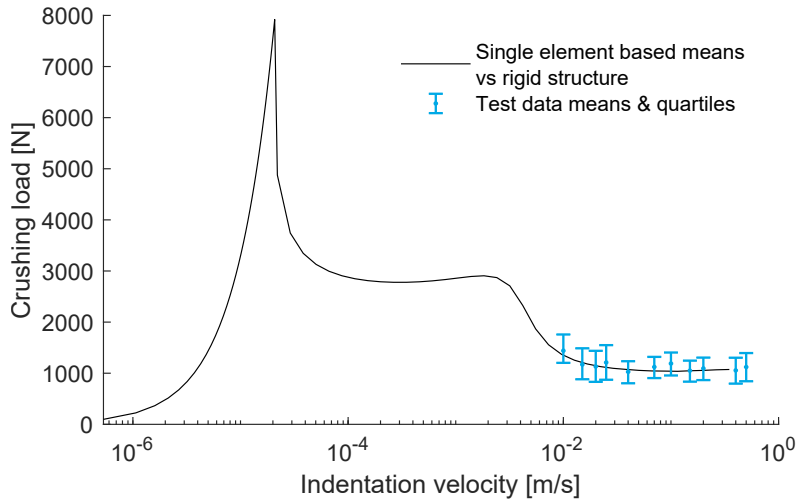


**Figure 1.4.** Model test data points shown.

$C_2$  has been derived from a  $v_t$  value found in literature. With a larger  $v_t$  (lower  $C_2$ ) the hump and the creep peak would move towards each other, changing the shape of the  $F_{mean}(v_{ice})$  relationship.

One practical consequence seen when inspecting Figure 1.4 is that it is not feasible to find  $C_2$  by any other means than measuring  $v_t$  and calculating  $C_2$ , or doing plastic relaxation tests. This is contrary to my earlier belief that it should be possible to calibrate  $C_2$  along with  $K_1$  and  $C_1$  if constant speed indentation tests can be done at speeds near  $v_t$ , or that  $v_t$  could be found by a slow enough indentation test. This belief partly relied on the previous measurements of  $v_t$ , which are significantly higher than our calculated finding.

It should be noted that Figure 1.4 is an apples to oranges comparison where the simulated data has no structural interaction (completely rigid structure representation) while the test data does contain load effects from interaction.

## B. Link to MATLAB code

<https://github.com/ecciv/thesis>

This repository contains the MATLAB codes used for simulation in this thesis. It may also contain some tikz code for generating figures, which may be used freely.

## C. Ram dimensions

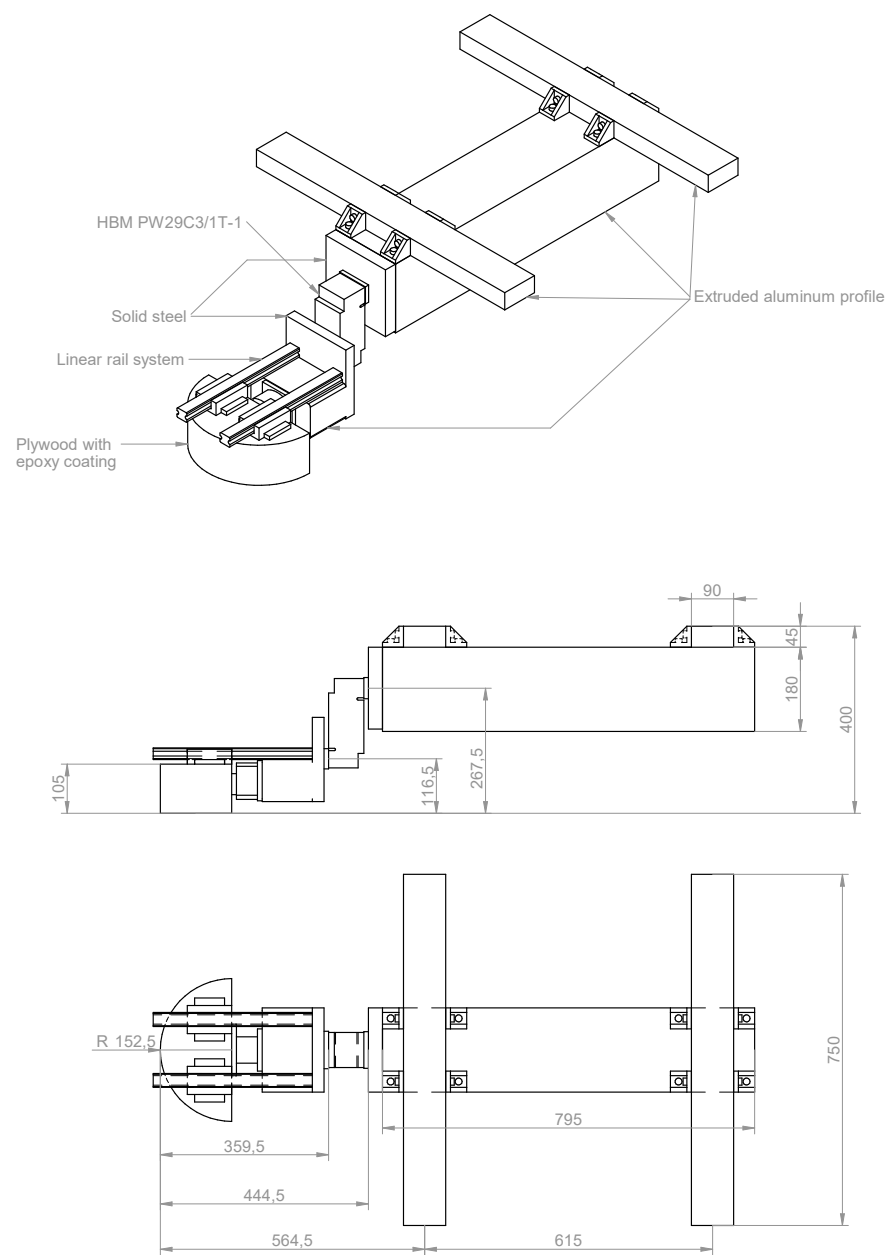


**Figure 3.1.** A schematic drawing of the ram.